Pergamon

Computers & Structures Vol. 50, No. 4, pp. 569–602, 1994

0045-7949/94 $6.00 + 0.00

MINIMUM-WEIGHT DESIGN OF A STIFFENED PANEL VIA PANDA2 AND EVALUATION OF THE OPTIMIZED PANEL VIA STAGS†

D. BUSHNELL and W. D. BUSHNELL

Department 93-30, Building 251, Lockheed Palo Alto Research Laboratory, 3251 Hanover St., Palo Alto, CA 94304, U.S.A.

(*Received* 29 *January* 1992)

Abstract—A minimum-weight design of a T-stiffened panel is found with the PANDA2 program. The panel, subjected to axial compression, in-plane shear, and normal pressure, is designed for service in its locally postbuckled state. A program called STAGSMODEL has been written for transforming output from PANDA2 to input for STAGS, a general-purpose nonlinear finite element code. STAGS is then used to evaluate the optimum design. Agreement between results obtained with PANDA2 and STAGS is reasonable for this very complex, very nonlinear problem. Therefore, PANDA2 qualifies as a preliminary design tool for panels operating in their locally postbuckled states.

INTRODUCTION

There is an extensive literature on the buckling and postbuckling behavior of stiffened plates and shells. This literature covers metallic panels and panels fabricated from laminated composite materials. Leissa [1] has gathered results from almost 400 sources on the buckling and postbuckling behavior of flat and cylindrical panels made of composite material with various stacking sequences and boundary conditions and subjected to various in-plane loads. The emphasis in his survey is on theoretical results, although some experimental results are included. He includes several examples in which the effect of transverse shear deformation is explored. Emphasis is given also to the effects of anisotropy on bifurcation buckling and on postbuckling behavior. Wiggenraad [2] surveys the literature on design of composite panels permitted to buckle locally under operating loads. Included in his survey are damage tolerance, fatigue, and optimization. Arnold and Parekh [3] emphasize in their survey and theoretical development the effect of in-plane shear load on the postbuckling behavior of stiffened, composite cylindrical panels. Surveys of earlier work on buckling of stiffened panels and shells appear in [4–6].

Among the foremost contributors of information about buckling of stiffened shells are Singer and his colleagues at the Technion in Haifa, Israel. In particular, the Baruch–Singer theory [7] for averaging the properties of stiffeners over a shell surface while retaining the important eccentricity effects has been incorporated into many widely used computer programs for the stress, vibration, and buckling analysis of stiffened shells.

The literature in the field of buckling of stiffened shells can be divided into three categories, one in which test results are emphasized, a second in which structural analysis is emphasized, and a third in which optimum designs are obtained. References [8–18] feature test results for plates, shells, and stiffeners made of laminated composite material; [19–26] feature structural analysis with structural properties fixed; and [27–38] feature structural analysis with optimum configurations sought in most cases via the widely used optimizers CONMIN or ADS, written by Vanderplaats and his colleagues [39–41].

This is just a sample of the literature on the subject. The reader is referred to the surveys given in [1–6] and references cited there for other sources.

CAPABILITIES OF PANDA2

PANDA2 finds minimum weight designs of laminated composite flat or curved cylindrical panels or cylindrical shells with stiffeners in one or two orthogonal directions. Stiffeners can be blades, tees, angles, or hats. Truss-core sandwich panels can also be handled. The panels or shells can be loaded by as many as five combinations of in-plane loads, edge moments, normal pressure, and temperature. The material properties can be temperature-dependent. The axial load can vary across the panel. The presence of overall (bowing) imperfections as well as local imperfections in the form of the local buckling mode are included. Constraints on the design include crippling, local and general buckling, maximum displacement under pressure, maximum tensile or

†Presented at 33rd AIAA SDM, Dallas, TX, 13–15 April 1992.

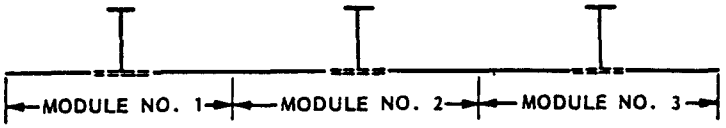

Fig. 1. T-stiffened panel with three modules.

compressive stress along the fibers and normal to the fibres in each lamina, and maximum in-plane shear stress in each lamina.

Local and general buckling loads are calculated with use of either closed-form expressions or with use of discretized models of panel cross sections. The discretized model is based on one-dimensional discretization similar to that used in the BOSOR4 computer code [42]. An analysis branch exists in which local postbuckling of the panel skin is accounted for. In this branch a constraint condition that prevents stiffener popoff is introduced into the optimization calculations. The postbuckling theory incorporated into PANDA2 is similar to that formulated by Koiter for panels loaded into the far-postbuckling regime [43].

PANDA2 can be run in five modes: simple analysis of a fixed design, optimization, test simulation, design sensitivity, and load-interaction. Plots of decision variables, margins, and weight vs design iterations can be obtained following use of PANDA2 in the optimization mode. Plots of user-selected behaviors vs load can be obtained following use of PANDA2 in the test-simulation mode. Plots of margins vs a user-selected design variable can be obtained following use of PANDA2 in the design sensitivity mode. Plots of in-plane load interaction curves and margins vs load combination number can be obtained following use of PANDA2 in the load-interaction mode.

There is a processor in the PANDA2 system that automatically generates an input file for the STAGS computer program [22, 23]. Thus, STAGS, which is a general-purpose nonlinear finite element analyzer, can easily be used to check the load-carrying capacity of panels designed with PANDA2.

Note that the theory on which PANDA2 is based is valid only if the panel is either unstiffened or, if stiffeners exist in either or both coordinate directions, there are several of them within the span of the panel. One cannot accurately determine the behavior of a panel with only one stiffener, for example. The panel, if axially stiffened, for example, has a 'field' of equally spaced, identical stringers.

In PANDA2 local buckling behavior is predicted from analysis of a single module which is assumed to repeat several times over the width of the panel, as shown for example in Fig. 1.

A panel module consists of one stiffener plus skin of width equal to the spacing between stiffeners. The single module is considered to be composed of segments, each of which has its own laminated wall construction. The cross-section of a single panel module is shown in Fig. 2 and the conventions used in PANDA2 for numbering the segments and the nodal points in the module are shown in Fig. 3. In Fig. 4 it is emphasized that the reference surface for each segment of the panel module is the middle surface of that segment. The segments are discretized as shown in Fig. 5. Details concerning the one-dimensional discretization (strip method) are provided in [42].

General instability is predicted from a model in which the stiffeners are 'smeared' in the manner of Baruch and Singer [7] over the width (stringers) and length (rings) of the panel. More details about PANDA2 appear in [44–47].

Improvements to PANDA2

Details about improvements to PANDA2 since publication of the original paper in 1987 are provided in [44, 45]. A summary of the most significant modifications and additions is provided here.

1. Plots of dimensions, objective, and design margins vs design iterations are generated by new processors, CHOOSEPLOT and DIPLOT, described in [44, 45]. Many of the plots in [44–47] and here were generated with the CHOOSEPLOT/DIPLOT processors. Plots can also be obtained of design margins

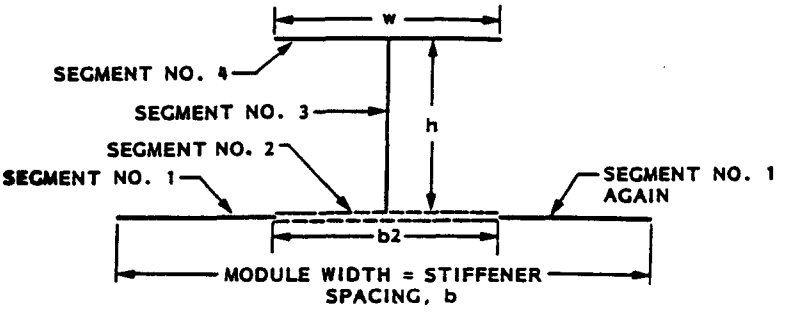

Fig. 2. A single panel module.

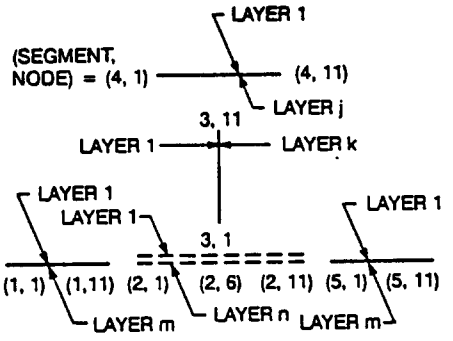

Fig. 3. Segment and nodal point numbering and layer numbering convention for a single panel module.

vs load and design margins vs any user-selected decision variable. Interaction curves for various combinations of in-plane loads N_x, N_y, N_{xy} can be obtained.

2. There is new flexibility with regard to the in-plane movability of the edges as the panel is loaded by normal pressure. Indeed, with movable boundaries of flat panels especially, the increased bowing and lack of development of average in-plane tension caused by bending can greatly reduce local buckling load factors, affecting the local postbuckling behavior and therefore the stress constraints that influence the evolution of the optimum design during optimization iterations.

3. New logic has been introduced to generate a 'knockdown' factor to compensate for the inherent unconservativeness of smearing stiffeners in the prediction of general (overall) and panel (between rings) instability, especially in cases where there is significant applied in-plane shear loading. The amount of knockdown is related (a) to the ratio of the wavelength of the buckles in the in-plane coordinate y normal to the stiffeners to the spacing b of the stiffeners, and (b) to the ratio of the applied in-plane shear load to the axial load.

4. Edge moments may be applied to the panel.

5. Temperature distributions may be applied to the panel and the material may be temperature-dependent. (Material must still behave linearly, however.)

6. If the panel is loaded by normal pressure, buckling and stress constraints are generated for conditions both at the midlength and at the ends of the panel. This modification is important because the very different distributions of axial compression over the skin–stringer cross-section cause very different buckling and stress behavior at these different axial locations. Behavioral constraint conditions corresponding to both panel midlength and panel ends may influence the evolution of the design during optimization iterations.

7. A new behavioral constraint condition based on bending–torsional buckling with a long axial wavelength has been introduced.

8. There may now be different boundary conditions for the prebuckling and bifurcation buckling phases of the problem. This modification is important for finding optimum designs of panels under normal pressure in which the panel being optimized spans

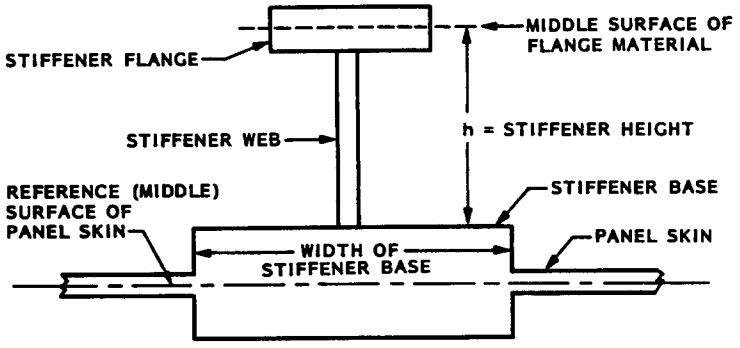

Fig. 4. Height of stiffener is measured from the top of the stringer base to the middle surface of the outstanding flange. Reference surface for all segments is the middle surface. Middle surface of the skin and stringer base is assumed to be continuous.

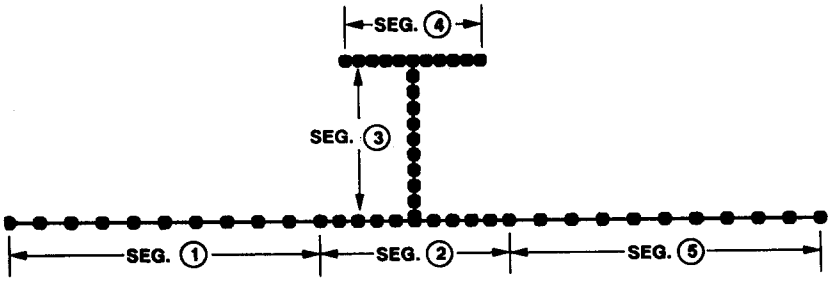

Fig. 5. Discretization of the T-stiffened panel module.

large rings. In the prebuckling phase the rings act like clamps, preventing edge rotation because of symmetrical behavior on either side of the ring. However, practical rings, especially those with open cross-sections, are likely to be too weak to prevent edge rotation that corresponds to twisting of the ring in the bifurcation buckling phase of behavior. Therefore, simple support conditions are often called for then.

9. If the panel is considered to be clamped in the prebuckling phase and if it is axially stiffened, its overall response to normal pressure is predicted from wide-beam bending theory in which the effect of axial compression is included. The theory is taken from Roark and Young [48]. At the midlength of the panel the change in curvature is given by

$$\text{Kappa}x\,(\text{midlength}) = p*(a/\sin(a) - 1)/[EI\,(\text{eff})*k**2] \quad (1)$$

in which

$$a = k*L/2, \quad k = \text{SQRT}[-N_x(\text{eff})/EI\,(\text{eff})], \quad (2)$$

where EI (eff) is the effective axial bending stiffness of the panel with smeared stringers and N_x(eff) is the effective axial resultant (positive for tension) acting on the panel.

The effective axial bending stiffness is obtained through a PANDA-type [4] general instability analysis of a wide panel clamped at its axially loaded ends with the effective axial stiffness of the panel skin and base under the stringer set equal to one half their nominal values in order to account for the diminished effective flange width of a beam with a wide flange. The quantity EI (eff) is calculated with use of the Euler buckling formula for a clamped–clamped column, P(Euler) = 4*pi**2*EI/L**2. Since P(Euler) = LAMBDA*ABS(N_x), the effective axial bending stiffness EI (eff) of the wide column is given by

$$EI\,(\text{eff}) = \text{LAMBDA}*\text{ABS}(N_x)*L**2/4*\text{pi}**2 \quad (3)$$

in which LAMBDA is the eigenvalue found from the PANDA-type buckling analysis [5] of the panel with smeared stiffeners.

The effective axial resultant, N_x(eff) = EBEAMR*N_x, accounts for the presence of in-plane shear N_{xy} combined with the axial load N_x. The factor EBEAMR is given by EBEAMR = LAMBDA/LAMBDA2, in which LAMBDA is the general instability buckling load factor with just N_x acting on the panel and LAMBDA2 is the general instability buckling load factor with both N_x and N_{xy} acting on the panel. Both LAMBDA and LAMBDA2 are computed from PANDA-type analyses [5].

The normal deflection at the midlength of the panel, W(pressure), is given by

$$w\,(\text{midlength}) = p*L*[\tan(a/2) - a/2]/[2*k*N_x(\text{eff})]. \quad (4)$$

At the ends of the panel the change in curvature is given by

$$\text{Kappa}x\,(\text{ends}) = -p*[1 - a/\tan(a)]/[EI\,(\text{eff})*k**2]. \quad (5)$$

For a panel with no axial load and with the panel skin considered to be fully effective as the beam–column bends, Equations (1), (4), and (5) assume the well-known forms

$$\text{Kappa}x\,(\text{midlength}) = (1/24)*p*L**2/C44 \quad \text{(neutral axis)} \quad (6)$$

$$w\,(\text{midlength}) = (1/384)*p*L**4/C44 \quad \text{(neutral axis)} \quad (7)$$

$$\text{Kappa}x\,(\text{ends}) = -(1/12)*p*L**2/C44 \quad \text{(neutral axis)}. \quad (8)$$

In the formulas above, p is the normal pressure, positive as shown in Fig. 8, page 490 of [38], L is the length of the panel between the large rings [which are not present as actual structures in the PANDA2 model, and C44 (neutral axis) is the bending stiffness per transverse arc length when the reference surface is the neutral plane in the x-direction].

The maximum web shear resultant, N_{xy} (due to pressure) is

$$N_{xy}(p) = (1/2)*p*L*b/h. \quad (9)$$

The beam bending model is used only for the deformation of the entire panel with smeared stiffeners. The local model for bending and stretching under pressure (single module) has not been changed, except that the user now has a choice as to whether the longitudinal edges are in-plane movable or not. The local model for behavior under pressure is described on pages 554–561 of [38].

10. More general linking expressions and inequality constraints based on the panel cross-section dimensions have been introduced into the DECIDE processor [38]. A general expression for a linked variable now has the form

$$\begin{aligned}(\text{linked variable}) &= C1*(\text{decision variable no. } j1) \\ &\quad + C2*(\text{decision variable no. } j2) \\ &\quad + C3*(\text{decision variable no. } j3) \\ &\quad + \text{etc (up to max. of 5 terms)} + C0 \end{aligned} \quad (10)$$

in which $C1$, $C2$, ... and $C0$ are constants. Inequality relations among variables may have either of the two forms

$$1.0 < f(v1, v2, v3, \ldots) \tag{11a}$$

or

$$1.0 > f(v1, v2, v3, \ldots), \tag{11b}$$

where the expression $f(v1, v2, v3, \ldots)$ has the form

$$f(v1, v2, v3, \ldots)$$
$$= C0 + C1*v1**D1 + C2*v2**D2 + C3*v3**D3$$
$$+ \ldots + \text{etc. (up to max. of 5 terms)}. \tag{12}$$

The variables, $v1$, $v2$, $v3$, ..., can be any of the variables that are decision variables or potential candidates for decision variables or linked variables.

11. Whereas formerly there were two choices for type of analysis: (1) optimization and (2) analysis of a fixed design at a fixed load, there are now also third, fourth, and fifth choices: (3) test simulation, (4) design sensitivity, (5) in-plane load interaction.

The choice of analysis type (1)–(5) is governed by a user-supplied index called ITYPE.

In the 'test simulation' mode the user supplies starting loads, load increments and the number of load steps. PANDA2 calculates the response of a panel of fixed design for a number of load steps until general instability is detected or until the maximum number of load steps specified by the user is reached.

In the 'design sensitivity' mode the user chooses a particular design variable and beginning and ending values of that variable. PANDA2 calculates the response with fixed loads and a number of panel designs in which the user-chosen design variable increases from its beginning value to its ending value. Margins can be plotted vs the chosen design variable.

In the 'in-plane load interaction' mode the user selects the type of load interaction: (N_x, N_y) with constant N_{xy}, or (N_x, N_{xy}) with constant N_y, or (N_y, N_{xy}) with constant N_x. The user also selects the ranges to be covered for the varying in-plane loads in the interaction and the number of load combinations for which to obtain margins. PANDA2 yields interaction plots for user-selected margins.

12. The assumed displacement field for calculation of PANDA-type buckling load factors has been modified for flat panels. In [5] a Rayleigh–Ritz method for obtaining bifurcation buckling loads of anisotropic flat and cylindrical panels is described. The assumed displacement field (u, v, w) for the buckling mode is given by eqns (50), page 552, of [5]

$$u = A\,[n2**2*m1*\sin(n1*y - m1*x)$$
$$+ n1**2m2*\sin(n2*y + m2*x)]$$
$$v = B\,[\quad n2*\sin(n1*y - m1*x)$$
$$+ n1*\sin(n2*y + m2*x)] \tag{13}$$
$$w = C\,[\quad \cos(n1*y - m1*x)$$
$$+ \cos(n2*y + m2*x)]$$

in which $n1$, $n2$, $m1$, $m2$ are given by

$$n1 = n + mc, \quad n2 = n - mc, \quad m1 = m + nd,$$
$$m2 = m - nd, \tag{14}$$

where c and d are the slopes of the buckling nodal lines as shown in Fig. 9 of [6]. The axial and circumferential wave indices m and n are defined as

$$m = M*\text{pi}/x\,(\text{max}), \qquad n = N*\text{pi}/y\,(\text{max}), \tag{15}$$

where M and N are the number of halfwaves over the axial length x (max) and the circumferential length y (max), respectively.

This formulation has been retained because it usually gives the best results for curved (cylindrical) panels, especially if the curved panel spans more than one radian. However, while comparing buckling loads for flat panels with unbalanced laminates from results obtained with the STAGS computer program [22, 23], especially when in-plane shear predominates, it was found that the following assumed displacement pattern yields better predictions

$$u = A\,[m1*\sin(n1*y - m1*x)$$
$$+ m2*\sin(n2*y + m2*x)]$$
$$v = B\,[n1*\sin(n1*y - m1*x)$$
$$- n2*\sin(n2*y + m2*x)] \tag{16}$$
$$w = C\,[\quad \cos(n1*y - m1*x)$$
$$- \quad \cos(n2*y + m2*x)].$$

13. A rather elaborate strategy has been introduced to obtain improved accuracy of buckling load factors for curved panels in which in-plane shear is a significant load component. Details of the strategy are included in the file called 'PANDA2 NEWS' [45], which forms part of the PANDA2 literature distributed with the program.

14. The local postbuckling theory, based on the work of Koiter [43], has been improved to allow for change in the axial wavelength of the local buckles as the panel is loaded further and further into the postbuckling regime. Details appear in [45].

15. Axial bending induced by neutral plane shift after local buckling has been introduced into the local postbuckling analysis.

16. The PANDA2 user may now obtain plots of extreme fiber strains vs load (test simulation mode) at several user-selected points in the panel module cross-section.

17. The move limits for decision variables during optimization cycles now depend to a certain extent on the value of the gradients of the behavioral constraint conditions.

18. The thermal buckling capability of PANDA2 has been improved. It is now possible to perform an ITYPE = 3 analysis (test simulation) with thermal loading only.

19. A PANDA2 processor called 'STAGSMODEL' has been written. This processor, using the PANDA2 database for a panel optimized by PANDA2, generates input files for the STAGS computer program and the STAGS postprocessor [22, 23]. With STAGSMODEL the user can check designs obtained from PANDA2 with a widely used, general-purpose, nonlinear static and dynamic finite element program.

20. Often when a stiffened panel is designed to withstand loads much higher than the local buckling load of the panel skin, there is 'secondary local buckling' or 'mode jumping'. That is, in tests of optimized panels bifurcation buckling of the already locally buckled panel skin has been observed at loads considerably above the initial local buckling load. If a panel is made of composite material which can delaminate relatively easily this secondary buckling, which usually occurs with a loud snapping noise, might well lead to early failure of the structure. Therefore, it is advantageous to be able to find optimum designs for which secondary buckling of the panel skin is unlikely to occur. Coding has been introduced into PANDA2 by means of which optimum designs of panels can be obtained for which secondary buckling may be postponed to loads that are higher than the design load.

21. PANDA2 now runs with UNIX-based operating systems.

CAPABILITY OF STAGS

STAGS (STructural Analysis of General Shells) is a finite element code for general-purpose nonlinear analysis of stiffened shell structures of arbitrary shape and complexity [22, 23]. Its capabilities include stress, stability, vibration, and transient analyses with both material and geometric nonlinearities permitted in all analysis types. Currently a new version of STAGS, scheduled for release through COSMIC in 1994, is under development. New enhancements include a higher order thick shell element, more advanced nonlinear solution strategies, accumulation of buckling modal imperfection shapes from previous linear or nonlinear runs, and more comprehensive post-processing features such as a link with PATRAN [49] and a sophisticated x–y plotting package called STAGSPP [52].

Research and development of STAGS by Brogan, Almroth, Rankin, Stanley, Cabiness, Stehlin and others of the Computational Mechanics Department of the Lockheed Palo Alto Research Laboratory has been under continuous sponsorship from U.S. government agencies and internal Lockheed funding for the past 20 years. During this time particular emphasis has been placed on improvement of the capability to solve difficult nonlinear problems such as the prediction of the behavior of axially compressed stiffened panels loaded far into their locally postbuckled states. STAGS has been extensively used worldwide for the evaluation of stiffened panels and shells loaded well into their locally postbuckled states. See [8], for example.

The following paragraphs about STAGS are taken from the STAGS literature written primarily by C. Rankin and H. Cabiness.

A large rotation algorithm that is independent of the finite element library has been incorporated into STAGS [50]. With this algorithm there is no artificial stiffening due to large rotations. The finite elements in the STAGS library do not store energy under arbitrary rigid-body motion and the first and second variations of the strain energy are consistent. These properties lead to quadratic convergence during Newton iterations.

Solution control in nonlinear problems includes specification of load levels or use of the advanced Riks–Crisfield path parameter that enables traversal of limit points into the post-buckling regime. Two loads systems with different histories (load sets A and B) can be defined and controlled separately during the solution process. Flexible restart procedures permit switching from one strategy to another during an analysis. This includes shifts from bifurcation buckling to nonlinear collapse analyses and back and shifts from static to transient and transient to static analyses with modified boundary conditions and loading. STAGS provides solutions to the generalized eigenvalue problem for buckling and vibration from a linear or nonlinear stress state.

Quadric surfaces can be modelled with minimal user input as individual substructures called 'shell units' in which the analytic geometry is represented exactly. 'Shell units' can be connected along edges or internal grid lines with partial or complete compatibility. In this way complex structures can be assembled from relatively simple units. Alternatively, a structure of arbitrary shape can be modelled with use of an 'element unit'.

Geometric imperfections can be generated automatically in a variety of ways, thereby permitting imperfection-sensitivity studies to be performed. For example, imperfections can be generated by superposition of several buckling modes determined from previous STAGS analyses of a given case.

A variety of material models is available, including both plasticity and creep. STAGS handles isotropic and anisotropic materials, including composites con-

sisting of up to 60 layers of arbitrary orientation. Four plasticity models are available, including isotropic strain hardening, the White Besseling (mechanical sublayer model), kinematic strain hardening, and deformation theory.

Two independent load sets, each composed from simple parts that may be specified with minimal input, define a spatial variation of loading. Any number of point loads, prescribed displacements, line loads, surface tractions, thermal loads, and 'live' pressure (hydrostatic pressure which remains normal to the shell surface throughout large deformations) can be combined to make a load set. For transient analysis the user may select from a menu of loading histories, or a general temporal variation may be specified in a user-written subroutine.

Boundary conditions (B.C.) may be imposed either by reference to certain standard conditions or by the use of single- and multi-point constraints. Simple support, symmetry, antisymmetry, clamped, or user-defined B.C. can be defined on a 'shell unit' edge. Single-point constraints which allow individual freedoms to be free, fixed, or a prescribed non-zero value may be applied to grid lines and surfaces in 'shell units' or 'element units'. A useful feature for buckling analysis allows these constraints to differ for the prestress and eigenvalue analyses. Lagrangian constraint equations containing up to 100 terms may be defined to impose multi-point constraints.

STAGS has a variety of finite elements suitable for the analysis of stiffened plates and shells. Simple four node quadrilateral plate elements with a cubic lateral displacement field (called '410' and '411' elements) are effective and efficient for the prediction of post-buckling thin shell response. A linear (410) or quadratic (411) membrane interpolation can be

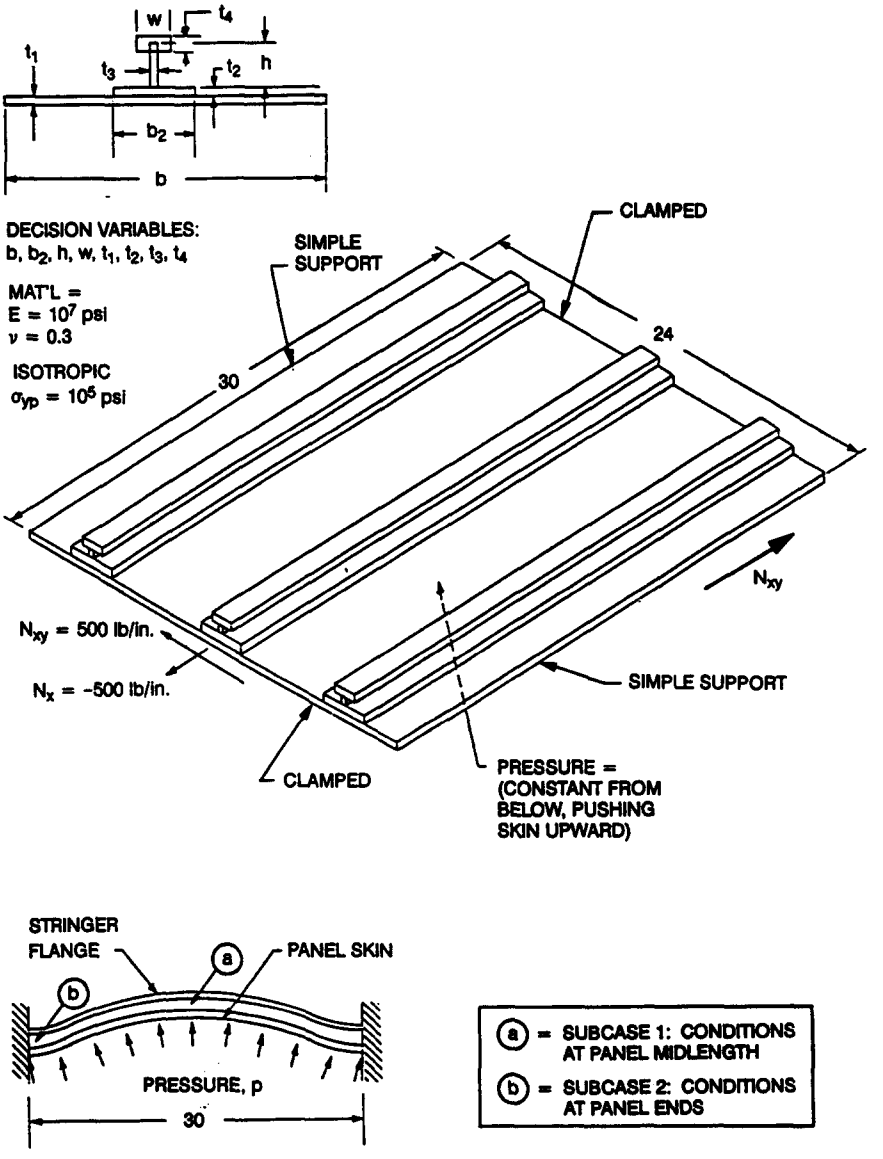

Fig. 6. Panel geometry, material properties, loading, and decision variables.

Table 1. Sequence of PANDA2 and STAGS execution commands for the optimum design of a T-stiffened flat panel clamped along its axially loaded edges and under combined axial compression, in-plane shear, and normal pressure with use of PANDA2 and evaluation of optimized panel with use of STAGS (Tables referred to here appear in [57])

Command	Input file	Table no.	Purpose of command
BEGIN	tee.BEG	Table 2	Set starting design; Matl prop. See Fig. 6 for configuration.
SETUP	none	none	Set up matrix templates.
DECIDE	tee.DEC	Table 3	Choose decision, linked variab., inequality constraints.

ITYPE = 1 (Optimization)

Use fully effective stiffness of panel skin for calculation of the load distribution over the panel module and for calculation of general buckling.

First, optimize with IQUICK = 1 ('Quick' analysis) and with local buckling NOT permitted (factors of safety, FSLOC, FSBSTR = 1.0).

Command	Input file	Table no.	Purpose of command
MAINSETUP	tee.OPT	Table 4	Establish loading, strategy, etc.
PANDAOPT	tee.OPT	Table 4	Batch run, IQUICK = 1
PANDAOPT	tee.OPT	Table 4	Batch run, IQUICK = 1
PANDAOPT	tee.OPT	Table 4	Batch run, IQUICK = 1
PANDAOPT	tee.OPT	Table 4	Batch run, IQUICK = 1

Next, continue optimization with IQUICK = 0 ('Long' analysis) and with local buckling NOT permitted (factors of safety, FSLOC, FSBSTR = 1.0). Use the fully effective panel skin stiffness.

MAINSETUP	tee.OPT	Table 5	Establish loading, strategy, etc.
PANDAOPT	tee.OPT	Table 5	Batch run, IQUICK = 0

Next, continue optimization with IQUICK = 0 ('Long' analysis) and with local buckling permitted (factor of safety, FSLOC = 0.1). Use the reduced effective panel skin stiffness.

MAINSETUP	tee.OPT	Table 6	Change FSLOC from 1.0 to 0.1 and change 'reduced effective stiffness' from 'N' to 'Y'.
PANDAOPT	tee.OPT	Table 6	Batch run, IQUICK = 0
PANDAOPT	tee.OPT	Table 6	Batch run, IQUICK = 0

An optimum design has been found. However, the stiffeners are rather closely spaced (b = 2.65 in). Use the CHANGE processor to increase b from 2.65 to 5.0 in and to increase the thickness of the panel skin, $t(1)$, from 0.03 to 0.05 in. Then use the DECIDE processor to raise the lower bound of b from 2.5 to 5.0 in.

Command	Input file	Table no.	Purpose of command
CHANGE	tee.CHG	Table 7	change b to 5.0 and $t(1)$ to 0.05 in
SETUP	none	none	setup matrix templates.
DECIDE	tee.DEC	Table 8	increase lower bound of b to 5.0 in

Continue optimization with IQUICK = 0 ('Long' analysis) and with YES local buckling permitted (factor of safety, FSLOC = 0.1). MAINSETUP input is the same as listed in Table 6, so it is not necessary to run MAINSETUP again.

Command	Input file	Table no.	Purpose of command
PANDAOPT	tee.OPT	Table 6	Batch run, IQUICK = 0
PANDAOPT	tee.OPT	Table 6	Batch run, IQUICK = 0

An optimum design has been found. However, in view of the very small change in minimum weight from the previously optimized design for which the stringer spacing was 2.65 in, it would be a good idea to raise further the lower bound of b and to continue optimization. Therefore, the CHANGE processor is used again, this time to increase b from 5.0 to 6.0 in and to increase the thickness of the panel skin, $t(1)$, from 0.037 to 0.05 in. Then use the DECIDE processor again, this time to raise the lower bound of b from 5.0 to 5.5 in.

Command	Input file	Table no.	Purpose of command
CHANGE	tee.CHG	Table 9	change b to 6.0 and $t(1)$ to 0.05 in
SETUP	none	none	setup matrix templates.
DECIDE	tee.DEC	Table 10	increase lower bound of b to 5.5 in

Continue optimization with IQUICK = 0 ('Long' analysis) and with YES local buckling permitted (factor of safety, FSLOC = 0.1). MAINSETUP Input is the same as listed in Table 6, so it is not necessary to run MAINSETUP again.

Command	Input file	Table no.	Purpose of command
PANDAOPT	tee.OPT	Table 6	Batch run, IQUICK = 0
PANDAOPT	tee.OPT	Table 6	Batch run, IQUICK = 0
PANDAOPT	tee.OPT	Table 6	Batch run, IQUICK = 0

Command	Input file	Table no.	Purpose of command
An optimum design has been found.			
Obtain plots of design variables, margins, objective versus iteration:			
CHOOSEPLOT	tee.CPL	not shown	Choose stuff to plot.
DIPLOT	none	none	Obtain plots (Figs 7, 8, 10)
CHOOSEPLOT	tee.CPL	not shown	Choose more stuff to plot.
DIPLOT	none	none	Obtain plots (Figs 9, 11)

ITYPE = 2 (Analysis of fixed design)

First, obtain a summary of information corresponding to the optimized panel.

Command	Input file	Table no.	Purpose of command
MAINSETUP	tee.OPT	Table 11 (top)	Set loads, etc. for fixed design.
PANDAOPT	tee.OPT	Table 11 (top)	Batch run for fixed design.
List the output (the blade.OPM file) from the batch run ...			
	tee.OPT	Table 11	Results for the fixed design. This is a summary, since the print control NPRINT = 0. The PANDA2 report, 'Annotated output ...' Ref. [53] contains much more output with added explanations.

ITYPE = 3 (test simulation of the optimized panel)

Perform test simulation on the optimized panel corresponding to SUBCASE 1 (conditions at the panel midlength). Obtain plots:

Command	Input file	Table no.	Purpose of command
MAINSETUP	tee.OPT	Table 12	Test simulation: panel midlength.
PANDAOPT	tee.OPT	Table 12	Batch run, test simulation
List the last part of the tee.OPI file:			
	tee.OPI	Table 13	Output from test simulation run.
Choose what to plot and obtain plots for the test simulation run:			
CHOOSEPLOT	tee.CPL	not shown	Choose stuff to plot.
DIPLOT	none	none	Obtain plots. Figs 12–15, 19
CHOOSEPLOT	tee.CPL	not shown	Choose more stuff to plot.
DIPLOT	none	none	Obtain plots. Fig. 16
CHOOSEPLOT	tee.CPL	not shown	Choose more stuff to plot.
DIPLOT	none	none	Obtain plots. Fig. 17
CHOOSEPLOT	tee.CPL	not shown	Choose more stuff to plot.
DIPLOT	none	none	Obtain plot. Fig. 18

Perform test simulation on the optimized panel corresponding to SUBCASE 2 (conditions at one end of the panel). Obtain plots:

Command	Input file	Table no.	Purpose of command
MAINSETUP	tee.OPT	Table 14	Test simulation: panel midlength.
PANDAOPT	tee.OPT	Table 14	Batch run, test simulation
Choose what to plot and obtain plots for the test simulation run:			
CHOOSEPLOT	tee.CPL	not shown	Choose stuff to plot.
DIPLOT	none	none	Obtain plots. Figs 20–22.

Evaluation of optimized panel
with the STAGS computer program

Next, use STAGSMODEL to set up various STAGS input models ...

Command	Input file	Table no.	Purpose of command
STAGSMODEL	tee.STG	Table 15	Set up linear bifurcation run. Results are shown in Fig. 24. Buckling mode No. 1 is used as an initial imperfection shape for the following nonlinear collapse run.
STAGSMODEL	tee.STG	Table 17	Set up nonlinear collapse run. Run stops at load step 7 because of bifurcations on primary equilibrium path. Results are shown in Figs 25–27. Buckling mode No. 2 is used as an additional initial imperfection shape for the following nonlinear collapse run.
STAGSMODEL	tee.STG	Table 18	Set up another nonlinear collapse run. Panel loads beyond the design load factor $PA = 1.0$. Results are shown in Figs 28–46.

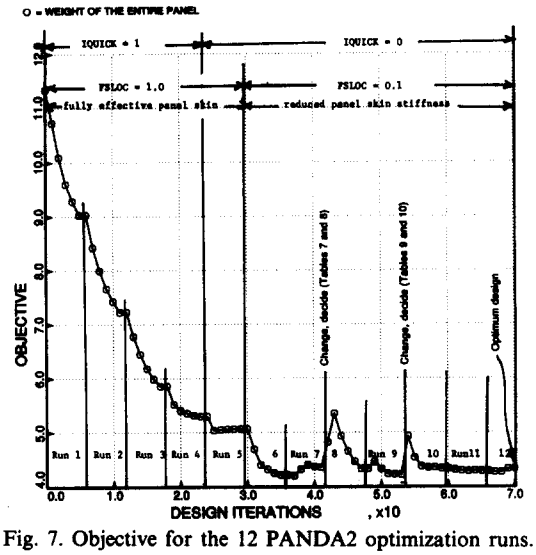

Fig. 7. Objective for the 12 PANDA2 optimization runs.

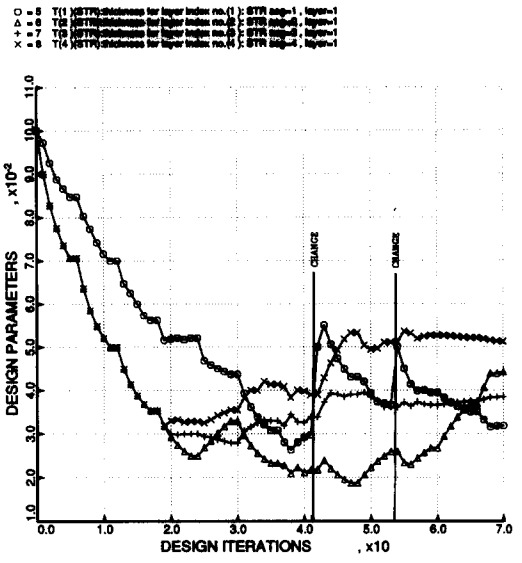

Fig. 9. Thicknesses for the 12 PANDA2 optimization runs.

selected. For thicker shells in which transverse shear deformation is important, STAGS provides the assumed natural strain (ANS) nine-node element (called '480' element). A two-node beam element compatible with the four-node quadrilateral plate element is provided to simulate stiffeners and beam assemblies. Other finite elements included in STAGS are described in the STAGS literature [51].

PANDA2-TO-STAGS MODEL GENERATION

A new PANDA2 processor, executed by the command 'STAGSMODEL', creates input files for STAGS corresponding to panel configurations optimized with PANDA2. With STAGSMODEL/STAGS the load-carrying capacity of optimum designs obtained by PANDA2 can be checked without the user having to spend time setting up elaborate finite element models for STAGS from directions in the STAGS user's manual. The STAGSMODEL processor can be used to create a succession of STAGS models by means of which bifurcation buckling behavior and nonlinear post-local-buckling behavior of a panel optimized by PANDA2 can be determined. This is a valuable feature because panels designed by the approximate methods used in PANDA2 can now easily be 'tested' by a widely used, rigorous, general, nonlinear finite element general-purpose program.

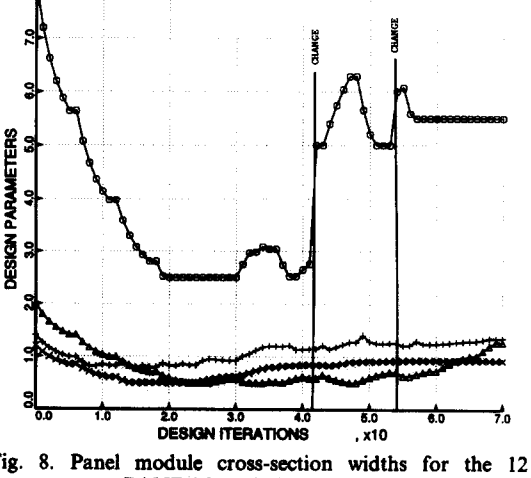

Fig. 8. Panel module cross-section widths for the 12 PANDA2 optimization runs.

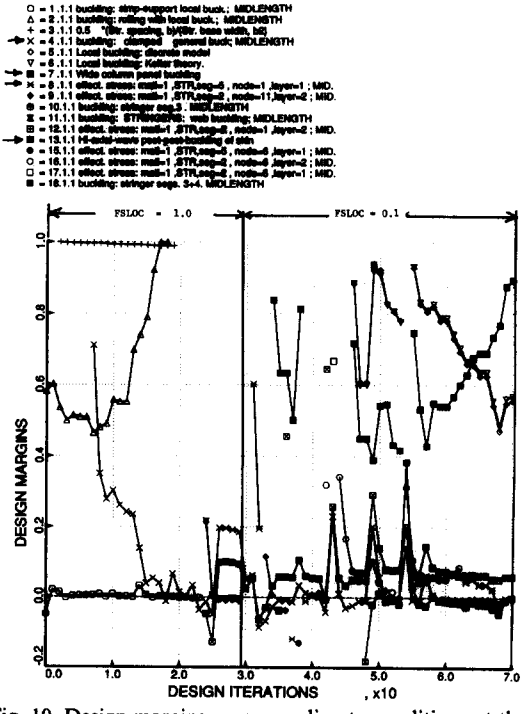

Fig. 10. Design margins corresponding to conditions at the panel midlength.

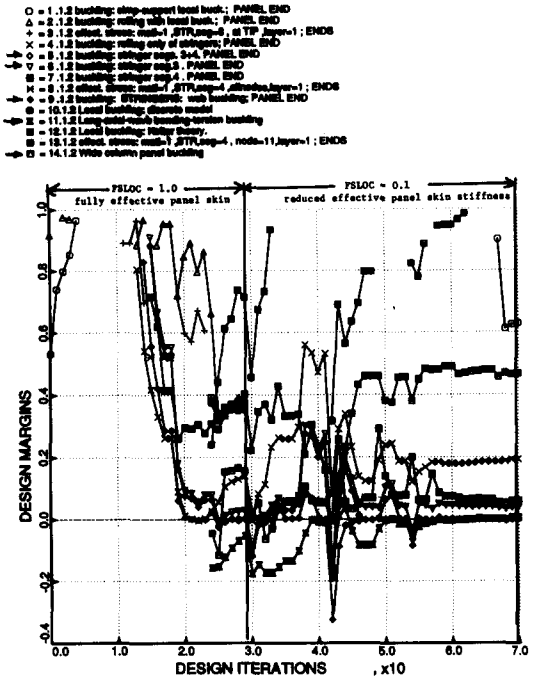

Fig. 11. Design margins corresponding to conditions at the panel ends.

The STAGSMODEL processor creates a finite element model of the part of a panel between adjacent rings. The stiffness along the axes of the rings is accounted for in the finite element model created by STAGSMODEL/STAGS. The panel can be loaded by any combination of uniform axial load N_x, uniform hoop load, N_y, uniform in-plane shear N_{xy}, and uniform normal pressure p.

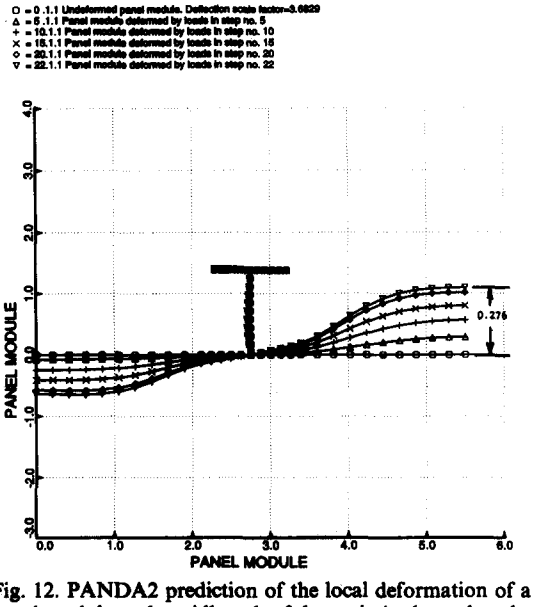

Fig. 12. PANDA2 prediction of the local deformation of a panel module at the midlength of the optimized panel as the load combination N_x, N_{xy}, p is increased.

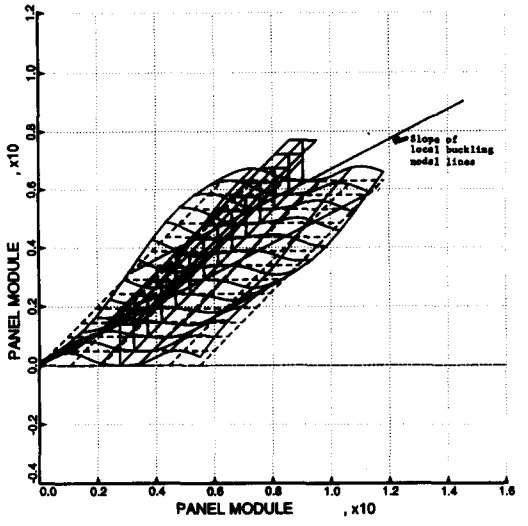

Fig. 13. PANDA2 prediction of the local deformation of a panel module corresponding to conditions at the panel midlength. One full axial wavelength of the local postbuckling pattern is shown.

Limitations in STAGSMODEL

Thermal loading and edge moments cannot yet be included. Truss-core sandwich panels cannot be handled. Also, if the panel is axially stiffened the axially loaded edges cannot rotate in either the prebuckling or bifurcation buckling phases of the analysis. The material must remain elastic. The loading/end shortening must be uniform.

Depending on a user-selected index, the normal projection of the two edges parallel to the stringers may be forced to remain straight or may be allowed to undergo in-plane warping (nonlinearly varying

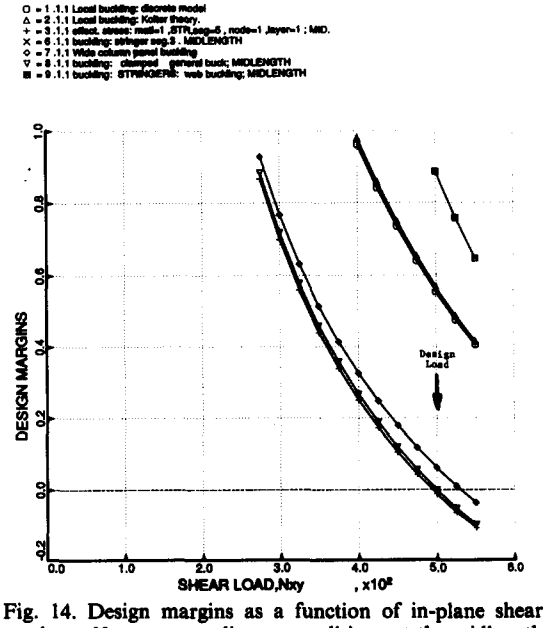

Fig. 14. Design margins as a function of in-plane shear resultant N_{xy} corresponding to conditions at the midlength of the optimized panel. Note that the three load components, N_x, N_{xy}, and p are always increased in proportion.

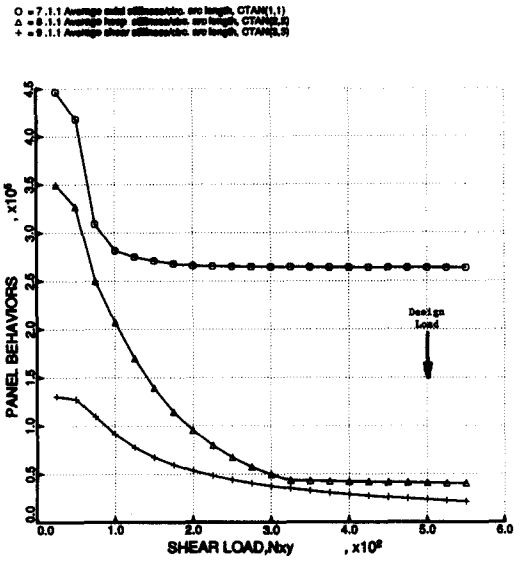

Fig. 15. PANDA2 prediction of average tangent stiffness of panel skin and stringer base at the panel midlength as the load combination N_x, N_{xy}, p is increased.

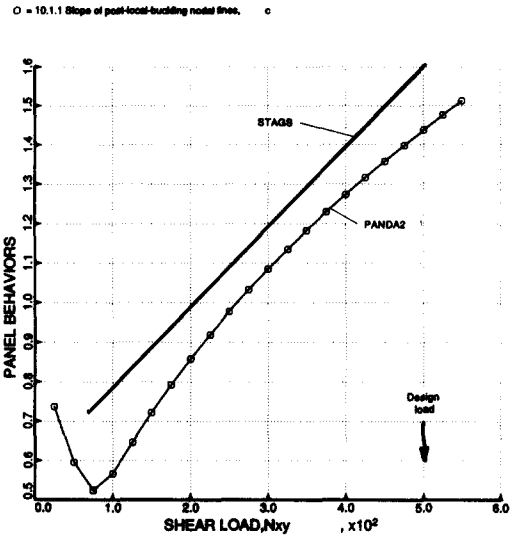

Fig. 17. PANDA2 and STAGS predictions of the slope of the nodal lines of the local buckles at the panel midlength as the load combination N_x, N_{xy}, p is increased.

circumferential displacement). At the axially loaded ends of the panel the cross sections of the stringers are not allowed to warp. In nonbifurcation phases of analyses the axial displacement u is zero at one end of the STAGS model and is uniform at the other end. The user chooses whether or not stringer sidesway is permitted at the axially loaded ends of the panel.

The entire STAGS model is created in what in STAGS jargon is called an 'element unit'. The stringer web(s) and outstanding flange are also modelled with finite elements. The line loads N_x, N_y, and N_{xy} and pressure p are modelled as nodal point loads. The user may choose to employ 410, 411, or 480 elements [51, 54–56]. If the user chooses 410 elements all segments of the panel are modelled with 410 elements except the bases under the stringers (Fig. 4), which are modelled with 411 elements. If the user chooses either 411 or 480 elements the entire panel is modelled with those elements.

NUMERICAL RESULTS FOR A T-STIFFENED PANEL

Optimization with PANDA2

Figure 6 shows the geometry, loading, boundary conditions, material properties, and decision variables. This case is described in [47]. However, at the time [47] was written the STAGSMODEL processor

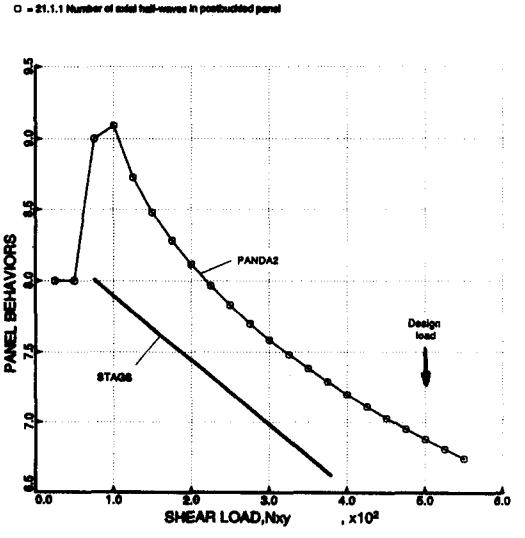

Fig. 16. PANDA2 and STAGS predictions of the number of axial halfwaves in the local postbuckling pattern corresponding to conditions at the panel midlength as the load combination N_x, N_{xy}, p is increased.

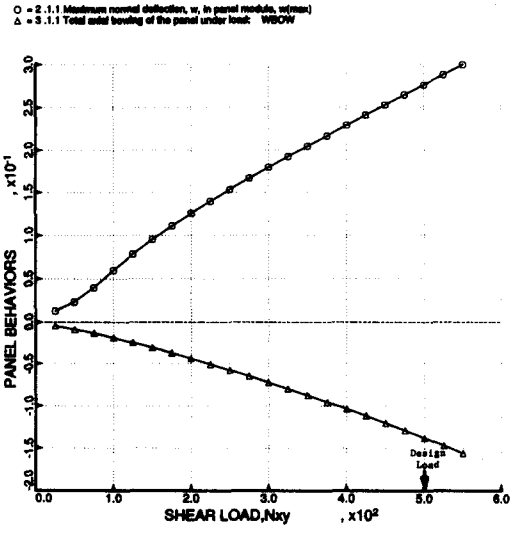

Fig. 18. PANDA2 predictions of the growth of the amplitude of the local buckles and of the overall axial bowing at the panel midlength as the load combination N_x, N_{xy}, p is increased.

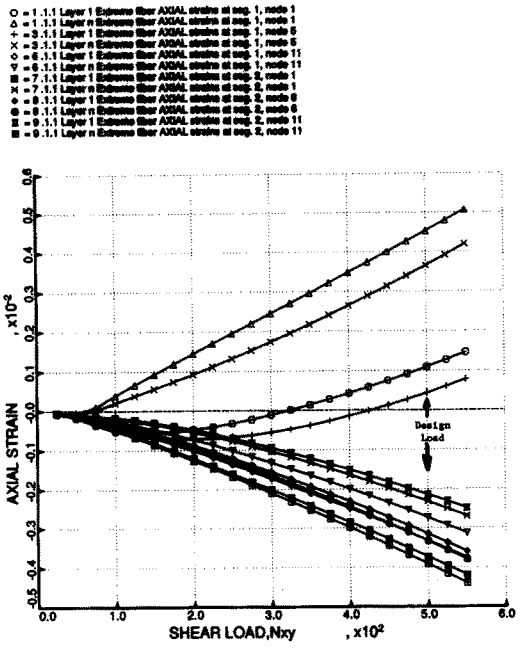

Fig. 19. PANDA2 prediction of axial strain in the panel skin and stringer base at the panel midlength as the load combination N_x, N_{xy}, p is increased.

was incomplete. During the past year many changes were made to PANDA2, mainly as a result of comparisons with STAGS predictions for a large variety of cases. These changes are documented in [45]. Because of these changes, the optimum design discussed next is different from that described in [47], though the initial design and loading are the same.

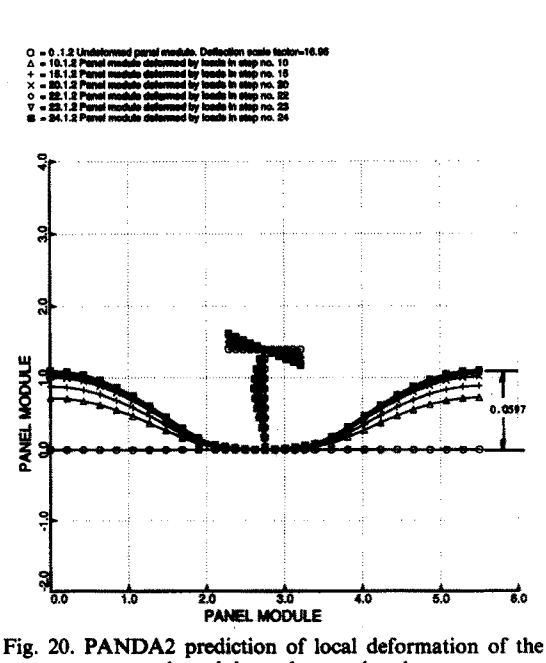

Fig. 20. PANDA2 prediction of local deformation of the panel module at the panel ends.

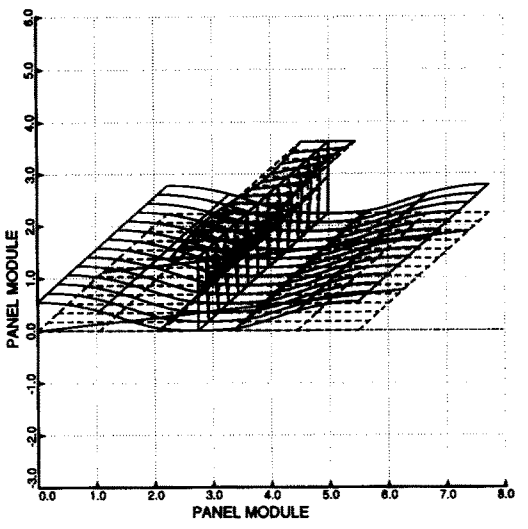

Fig. 21. Three-dimensional view of the local deformation of the panel module near the panel ends.

The T-stiffened panel is loaded by

axial compression: $N_x = -500$ lb/in
in-plane shear: $N_{xy} = 500$ lb/in
normal pressure: $p = 5$ psi.

The three loads, N_x, N_{xy}, p, are increased proportionally, that is, they are all in load set A.

The material is isotropic and aluminum-like. The yield stress has been set very high (100 ksi) so that optimization of the panel leads to a configuration that is loaded very far into the locally postbuckled state. This provides a challenging test of both PANDA2 and STAGS.

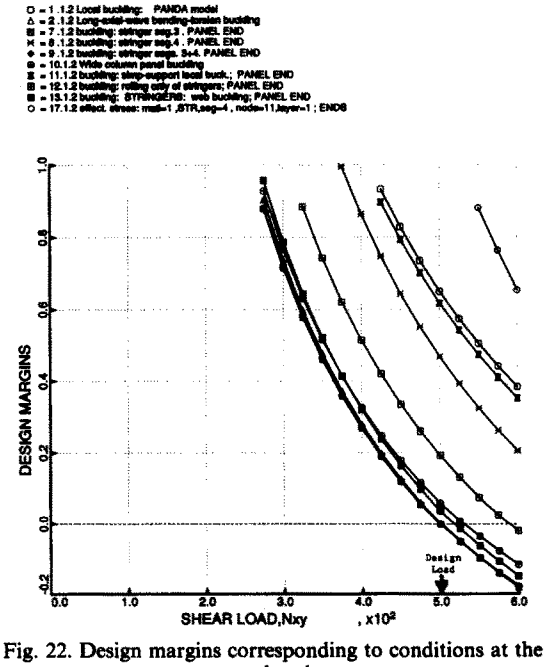

Fig. 22. Design margins corresponding to conditions at the panel ends.

It is emphasized that although this example is for a simple wall construction, PANDA2 and STAGS are capable of handling laminated composite panels.

Evolution of the design during optimization iterations is governed by conditions at the midlength and at the ends of the panel. Because the normal pressure bends the panel upward, at the midlength of the panel the skin is compressed more than the stringers. The reverse holds at the panel ends. At the midlength of the panel the design is constrained mainly by high local stresses generated by bending of the panel skin loaded far into the postbuckling regime. At the ends of the panel, where the stringers are compressed more than the panel skin, the design is constrained by various local buckling modes of the stringer segments and by overall bending–torsion buckling of the stringers.

The decision variables of the design problem are identified in Fig. 6. Table 1 lists the runstream that yielded the optimum design via PANDA2 and the evaluation of this design via STAGS. The files containing input data for the BEGIN, DECIDE, MAINSETUP, CHANGE, and STAGSMODEL PANDA2 processors are listed in Tables 2–10, 12, 14, 15, 17, and 18 of [57].

As indicated in Fig. 7 the final optimum design is obtained in 12 runs of six iterations each, except for the final run, in which convergence was obtained in five iterations. (Actually, there are five iterations in the first 11 runs and four in the final run. The first

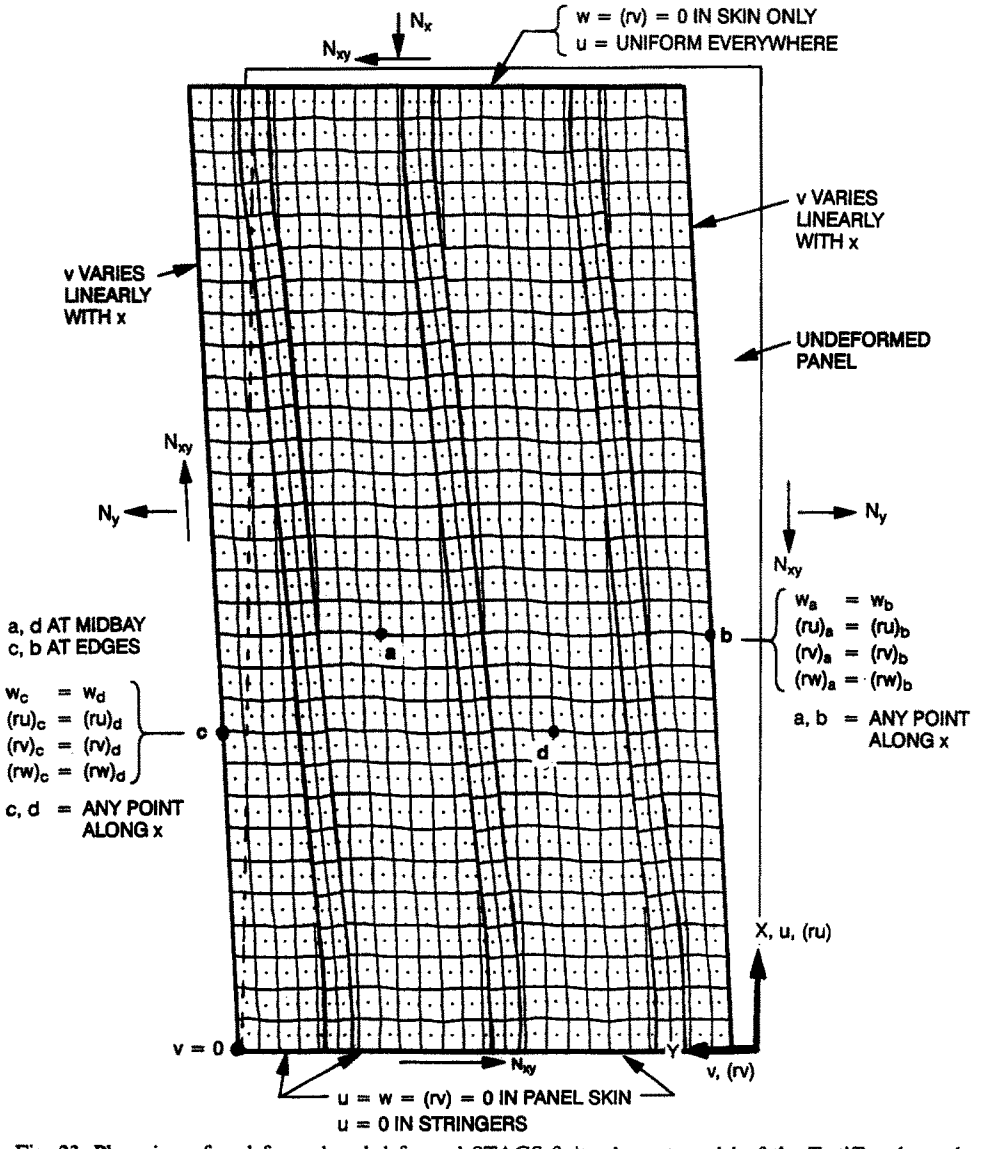

Fig. 23. Plan view of undeformed and deformed STAGS finite element model of the T-stiffened panel. The in-plane loading components N_x and N_{xy} are shown, as well as the boundary conditions for the case in which the two edges parallel to the stringers (longitudinal edges) are prevented from warping in the plane of the panel skin.

'iteration' of each run is simply a restatement of the final design obtained in the previous run.)

Two optima are obtained. The first corresponds to a panel in which local buckling is *not* permitted. (Local buckling is prevented by setting the factor of safety for local buckling, FSLOC, equal to a number greater than unity). The weight of this optimum design, 5.07 lb, is determined after run 5. The dimensions of the panel module cross-section (Fig. 6, top left) are: $b = 2.5$ in, $b2 = 0.582$ in, $h = 0.925$ in, $w = 0.615$ in, $t(1) = 0.0437$ in, $t(2) = 0.0329$ in, $t(3) = 0.0279$ in, $t(4) = 0.0355$ in.

The final optimum is about 15% lighter and is obtained from an analysis in which local postbuckling *is* permitted. (Local buckling is permitted if the factor of safety for local buckling, FSLOC, is set equal to a number less than unity. In this case FSLOC = 0.1.) The final dimensions of the panel module cross-section are: $b = 5.5$ in, $b2 = 1.28$ in, $h = 1.35$ in, $w = 0.926$ in, $t(1) = 0.0318$ in, $t(2) =$

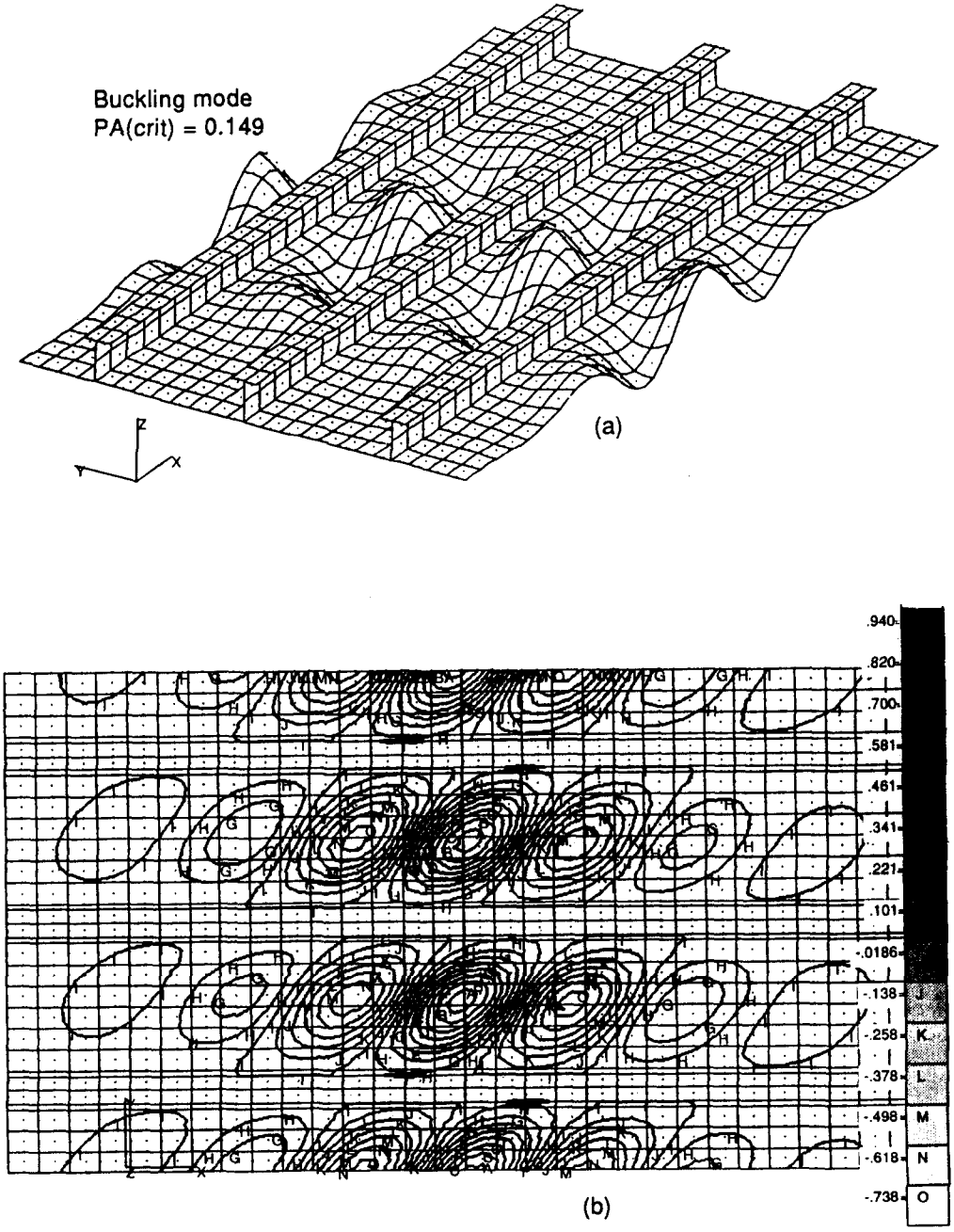

Fig. 24. STAGS prediction of buckling mode and critical load factor from linear bifurcation buckling theory. This mode shape is used as an initial imperfection in the nonlinear equilibrium STAGS analysis. (a) Three-dimensional view of buckling mode; (b) contour plot that shows the slope of the nodal lines of the local buckling mode and its axial wavelength.

Table 2. Sequence of STAGSMODEL/STAGS runs required to complete a case

Run No.	Name of run	Purpose of the run
1	STAGSMODEL	Create STAGS input file for linear buckling analysis (INDIC = 1). Purpose is to create imperfection shapes to use in the first nonlinear run (the first run with analysis type INDIC = 3). Example of input data: Table 15.
2	STAGS	Obtain local buckling modes from STAGS to use as imperfections in the next STAGS run. Example of results: Fig. 24(a,b).
3	STAGSMODEL	Create STAGS input file for nonlinear collapse analysis (INDIC = 3). Amplitudes of imperfections must be included as input data in this run. Example of input data: Table 17.
4	STAGS	Perform 1st nonlinear collapse analysis. Failure of convergence may occur at a load smaller than the design load (load factor PA = 1.0), or the Riks path may reverse upon itself. If bad things happen in this run, which is likely, go on. Otherwise, the nonlinear analysis is complete. In the particular case explored here the nonlinear analysis failed to converge beyond Load Step 7. When this happens STAGS automatically computes a user-specified number of eigenvalues and modes for the panel as loaded at the last step for which a converged solution was obtained. Example of results: Figs 25–27.
5	STAGSMODEL	If the previous nonlinear collapse run ends without computing eigenvalues and modes, create a STAGS input file for bifurcation buckling with nonlinear prebuckling analysis (INDIC = 4). Choose as a starting load that which corresponds to the maximum load for which convergence was reliably obtained in the previous STAGS run and for which no roots had been skipped. (Inspect the STAGS output file called *.out2 to find out what happened in the previous STAGS nonlinear run.)
6	STAGS	Perform bifurcation buckling with nonlinear prebuckling. The purpose of this run is to obtain additional imperfection shapes that will (it is hoped!) eliminate the near-singularity that caused the difficulty in the previous nonlinear (INDIC = 3) STAGS run.
7	STAGSMODEL	Create STAGS input file for the second nonlinear run (INDIC = 3). It is safest to restart the case from the zeroth load step, even though this takes more computer time. Example of input data: Table 18.
8	STAGS	Perform the second nonlinear collapse analysis. If no difficulties occur below the collapse load the case is finished. If there are difficulties repeat the (INDIC = 4, INDIC = 3) sequence of STAGSMODEL/STAGS runs until enough imperfections have been accumulated to eliminate lack of convergence and/or Riks path reversal. Example of results: Figs 28–47

0.0442 in, $t(3) = 0.0384$ in, $t(4) = 0.0512$ in. The final weight of the panel is 4.33 lb.

In the first four runs the index IQUICK is unity, which means that all buckling analyses are performed with use of PANDA-type (closed form) models, as described in [5] with the modifications listed above in the 'Improvements to PANDA2' section. The remaining runs are performed with IQUICK = 0, which means that local buckling and wide-column buckling are performed with the discretized single panel module model shown in Fig. 5.

Plots of the decision variables, b, $b2$, h, w, $t(1)$–$t(4)$, vs design iteration appear in Figs 8 and 9. For runs 10–12 the minimum allowable stringer spacing b was 5.5 in. This rather high minimum allowable value was imposed for the following reasons:

1. The optimum panel weight is very insensitive to stringer spacing in the range $2.5 < b < 5.5$ inches, but if b is not constrained it tends toward the lower end of this range.

2. The post-local-buckling behavior becomes more interesting as b is increased because the panel state at the design load combination, $N_x = -500$ lb/in, $N_{xy} = 500$ lb/in, $p = 5$ psi, is further into the post-local-buckling regime for a larger value of b.

3. Fewer finite elements in the STAGS model are required for adequate convergence to the equilibrium state in the local postbuckling regime because the

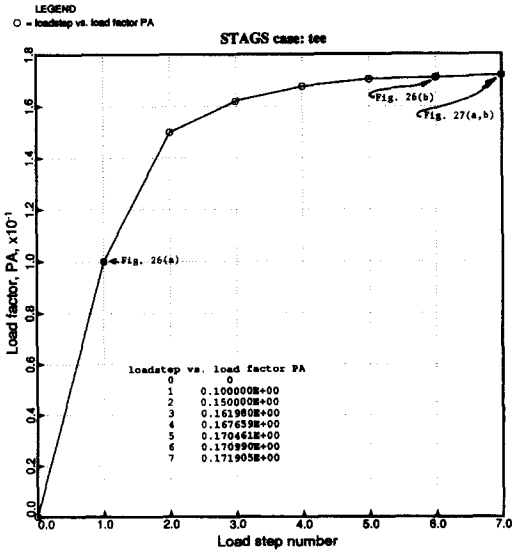

Fig. 25. Results from the first nonlinear equilibrium run with STAGS. The run stopped at load step 7 because of a bifurcation on the primary load path.

number of axial halfwaves in the local buckling pattern decreases as b increases.

Figure 10 shows the margins corresponding to conditions at the midlength of the panel, where the panel skin is axially compressed more than the outstanding flanges of the stringers. Figure 11 shows the margins corresponding to conditions at the ends of the panel, where the reverse holds.

Panel midlength. At iteration 30, which corresponds to the optimum design for a panel in which local buckling is *not* permitted (FSLOC = 1.1), the critical margins are local buckling and general or wide column buckling. At the final optimum design, for which local buckling *is* permitted (FSLOC = 0.1), the critical margins are general instability and wide column buckling, maximum effective stress, and high-axial-wavenumber bifurcation buckling of the locally postbuckled panel.

In Fig. 10 the margin labelled 'Hi-axial-wave post-postbuckling of skin' pertains to paragraph 20 of the section, 'Improvements to PANDA2'. This margin is generated by performance of a local buckling analysis of the discretized single panel module in which the distributions of resultants N_x, N_y, and N_{xy} from the Koiter postbuckling analysis are used rather than the initial prebuckling distributions. Secondary buckling occurs with about twice the number of axial halfwaves that occur in the initial local buckling analysis. Usually the maximum normal displacement in the secondary buckling mode occurs near the stringers. Secondary buckling is caused primarily by

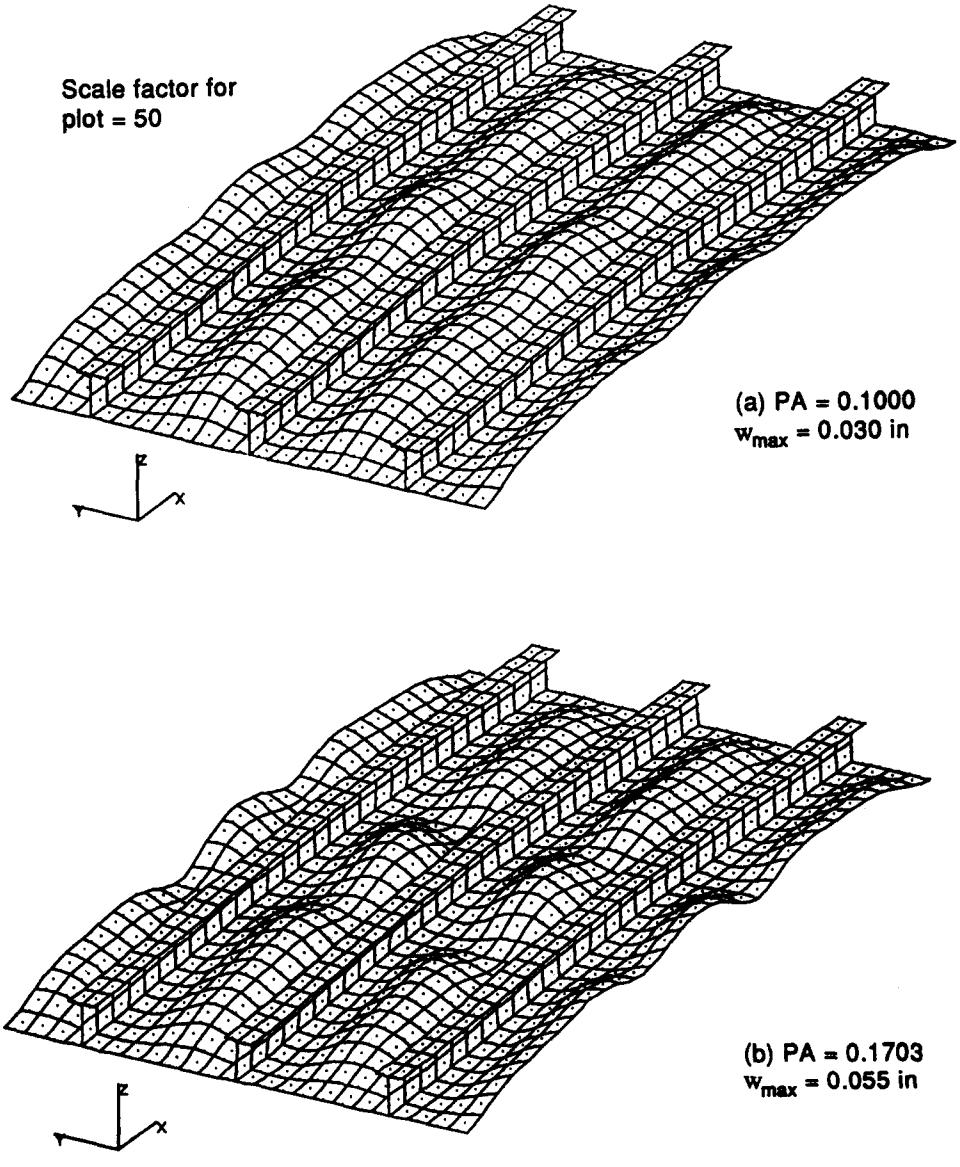

Fig. 26. Deformed panel at (a) load factor 0.1, (b) load factor 0.17. The 'pillowing' between stringers is caused by the normal pressure. The presence of the initial imperfection shown in Fig. 24 gives rise to the axial nonuniformity of the 'pillowing'.

redistribution of the axial load N_x away from the region midway between stringers and toward the stringers as the skin buckles in the local postbuckling regime. The recent introduction of the secondary buckling constraint is one factor causing the optimum design of the T-stiffened panel to be different here from that described in [47].

Note that maximum stress constraints are active only at the midlength of the panel. This makes sense because the pressure bends the panel so that the skin at the panel midlength is loaded far into the local postbuckling regime.

Panel ends. At iteration 30 (FSLOC = 1.1) the critical margins are buckling of stringer segments 3 and 4 (web and flange) together, buckling of the stringer web, and long-axial-wave bending–torsion buckling. At the final optimum design (FSLOC = 0.1) the critical margins are the same, with the addition of wide-column buckling.

Table 11 of [57] presents a summary of results for the final optimum design. According to PANDA2, the panel skin buckles at the midlength at a load of about 15% of the design load (local buckling load factor = 0.15).

Test simulation of the optimized panel with PANDA2

The input data are listed in Table 12 of [57].

Table 13 of [57] and Figs 12–19 pertain to conditions at the midlength of the panel (subcase 1) and Figs 20–22 pertain to conditions at the ends of the panel (subcase 2). Although most of these figures show plots of behaviours vs the applied in-plane shear resultant N_{xy}, bear in mind that the three load components, N_x, N_{xy}, and p, are being increased

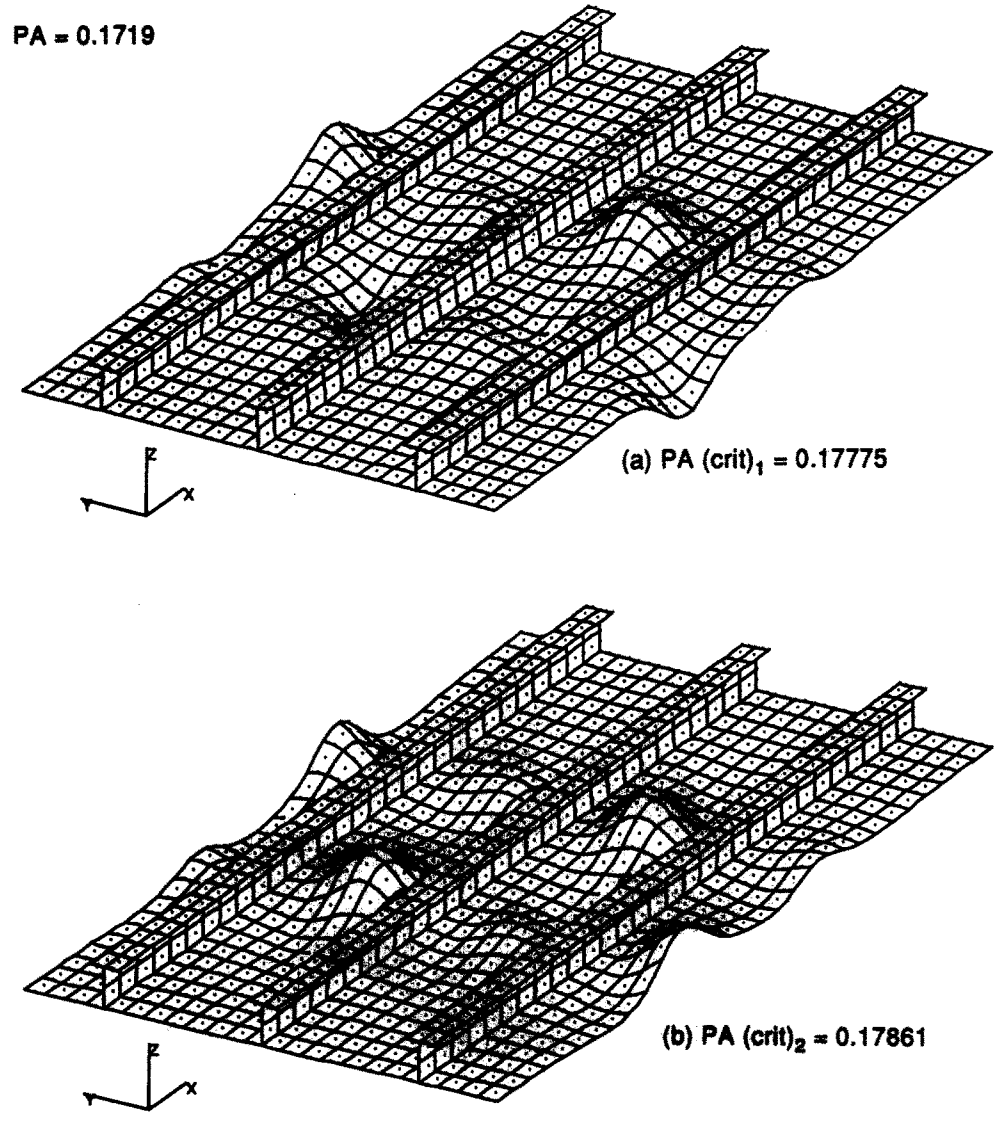

Fig. 27. Eigenmodes and critical load factors for the panel at load step 7, load factor $PA = 0.1719$. (a) First mode: critical load factor, PA (crit) = PA (1 + eigenvalue) = 0.17775; (b) second mode: critical load factor, PA (crit) = 0.17861. The second mode is to be used as an additional initial imperfection shape with amplitude given by −0.002 in the next nonlinear STAGS run.

proportionally in the test simulation (ITYPE = 3) mode.

Panel midlength. Table 13 of [57] presents a summary of the state of the panel for conditions at the panel midlength. It should be emphasized that in the PANDA2 analysis conditions that exist at the panel midlength (subcase 1) are assumed to exist over the entire length of the panel when subcase 1 results are being calculated, and conditions that exist at the panel ends (subcase 2) are assumed to exist over the entire length of the panel when subcase 2 results are being calculated. For example, the average axial strain of the reference surface of the panel skin, $e1$, which is computed from the Koiter theory as described in [38], is assumed to be independent of the axial coordinate, x. Therefore, according to PANDA2, the end shortening is $e1$ times the panel length, L (called 'AXIAL' in the PANDA2 output). In this case, since the panel is clamped at its axially loaded ends and therefore experiences changes in sign of the axial curvature as it deforms under the uniform pressure, the end shortening calculated corresponding to conditions at the midlength of the panel will be overestimated and the end shortening calculated corresponding to conditions at the ends of the panel will be underestimated.

Figure 12 shows how the panel module cross-section deforms as the panel is loaded further and further into its locally postbuckled state. The normal deflection is larger in the panel skin on the right side of the stringer than on the left side because local deformations from the normal pressure and from local buckles reinforce each other there, whereas these deformations tend to cancel each other on the left side of the stringer at the particular axial station represented in Fig. 12. (The deformed cross-section varies in the axial direction because the local postbuckling deformation has many axial halfwaves whereas the local deformation caused by the normal pressure is prismatic.)

Figure 13 depicts a '3-D' view of a portion of the length of the panel module that corresponds to one full wave of the local postbuckling pattern.

Figure 14 shows all margins less than unity. At the design load combination, $N_x = -500$ lb/in, $N_{xy} = 500$ lb/in, $p = 5.0$ psi, the three critical margins involve effective stress, general instability, and wide-column buckling. The 'high-axial-wave post-post buckling' margin is not computed in the test simulation mode.

Figure 15 depicts the average tangent stiffness components of the locally postbuckled panel skin and stringer base. These quantities affect the general instability predictions because at the load corresponding to general instability the panel skin has a smaller effective stiffness because it is buckled. This phenomenon is called 'modal interaction' in the literature on buckling of stiffened panels. Note that because there is assumed in this analysis to be an initial local imperfection that has an amplitude approximately equal to one-tenth the thickness of the panel skin midway between stringers, the tangent stiffness components start to decrease well below the load corresponding to local bifurcation buckling ($0.15 \times 500 = 75$ lb/in). This is because the initial imperfection, which is assumed to be in the form of the critical local buckling mode, starts to grow as soon as *any* load is applied.

Figure 16 shows how the number of axial halfwaves along the 30-in length of the panel varies as the panel is loaded into the postbuckling regime. Figure 17 shows how the slope of the nodal lines of the local buckles varies in the post-local-buckling regime. At bifurcation the critical number of halfwaves is eight and the slope of the nodal lines of the local buckles is about 0.45. Except in the immediate neighborhood of the local buckling load, as the panel is loaded further and further into its postbuckled state the number of axial halfwaves decreases and the slope of the nodal lines increases. Results from STAGS, to be discussed below, confirm the PANDA2 predictions of these changes in the configuration of the local buckles.

Note that in PANDA2 the boundary conditions at the axially loaded edges of the panel are assumed to have no effect on buckling. Therefore, the critical axial wavelength of the local postbuckling pattern is free to change in a continuous manner. Actual panels do not behave in this way unless there is a very large number of local buckles along the length of the panel.

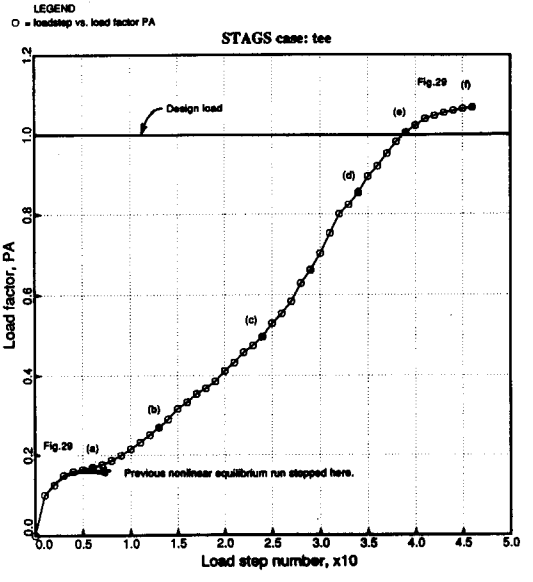

Fig. 28. Results from the second nonlinear STAGS run. With the new imperfection shape shown in Fig. 27(b) added to that from the linear buckling analysis shown in Fig. 24, the load factor PA could be increased well above the point where convergence failure occurred in the previous nonlinear STAGS run, indeed PA could be increased above the design load factor, $PA = 1.0$, without difficulty.

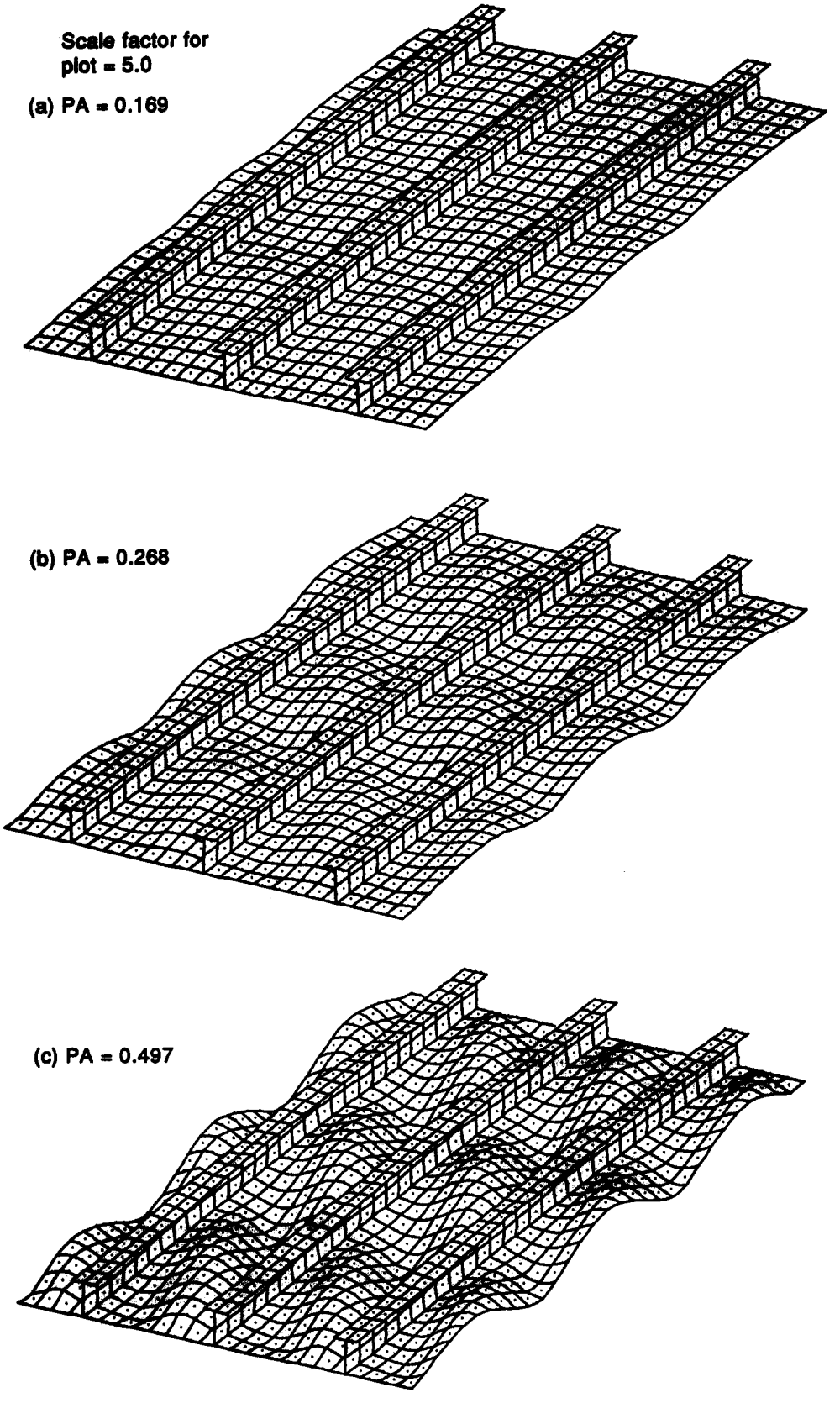

Fig. 29a, b and c.

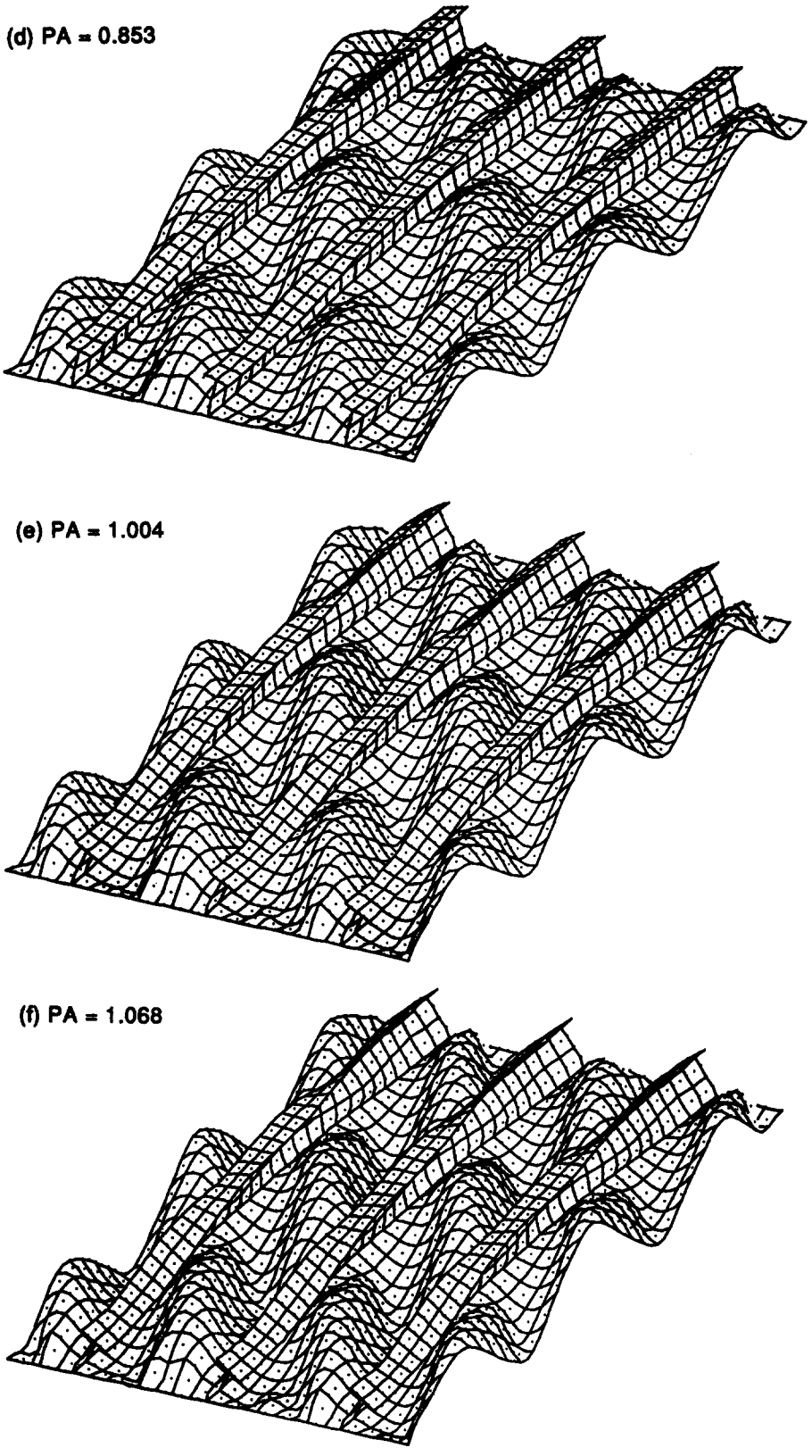

Fig. 29. How the panel deforms with increasing load factor *PA*.

In actual panels the wavelength of the locally postbuckled panel may vary along the length and/or the number of axial waves may change suddenly as the load is increased (mode jumping).

Figure 18 displays the growth in amplitude of the local buckles (top curve) and the growth in axial bowing (bottom curve) as functions of the applied in-plane shear load N_{xy}. The axial bowing arises from two sources: the normal pressure and the redistribution of axial resultant N_x after local buckling. According to PANDA2, at the design load ($N_x = -500$ lb/in; $N_{xy} = 500$ lb/in; $p = 5$ psi), about 0.101 in of the axial bowing arises from the normal pressure acting on a panel that is preloaded by axial compression N_x and in-plane shear N_{xy}, and about 0.038 in of the axial bowing arises from redistribution of the axial resultant N_x in the local postbuckling regime.

Extreme fiber axial strains in the panel skin at the panel midlength are plotted vs applied load in Fig. 19. Locations of (segment, node) pairs are identified in Figs 3 and 5.

Panel ends. The input data are listed in Table 14 of [57].

Figures 20–22 show conditions at the ends of the panel. At the ends of the panel the stringer parts are axially compressed more than the panel skin. Therefore, the local deformations of the single panel module are very different from those at the panel midlength depicted in Figs 12 and 13. For example, the deformation in the panel skin is caused entirely by the normal pressure and is therefore uniform in the axial direction, as shown in Fig. 21. (It is assumed in PANDA2 that the local deformation caused by normal pressure is prismatic. See Fig. 56 on p. 555 [38].) Deformation of the stringer parts is caused by local buckling of the stringer web and flange. PANDA2 predicts that local buckling of the stringers in the mode shown in Figs 20 and 21 occurs at a load factor of about 1.5. This buckling mode has 19 axial halfwaves along the 30-inch length of the panel.

Note that in this case there is a more critical stringer buckling mode corresponding to conditions at the ends of the panel: bending–torsion buckling of the stringer and attached panel skin. As listed on p. 3 of Table 11 in [57], the load factor for this mode of buckling is 1.1 and the number of axial halfwaves is 2. In PANDA2 bending–torsion buckling of the stringers is considered to be a type of general instability rather than local buckling. That is why the bending–torsion mode is not plotted as shown in Figs 20 and 21 and that is why the local postbuckling analysis is performed for the more localized high-axial-wavenumber mode, even though this mode

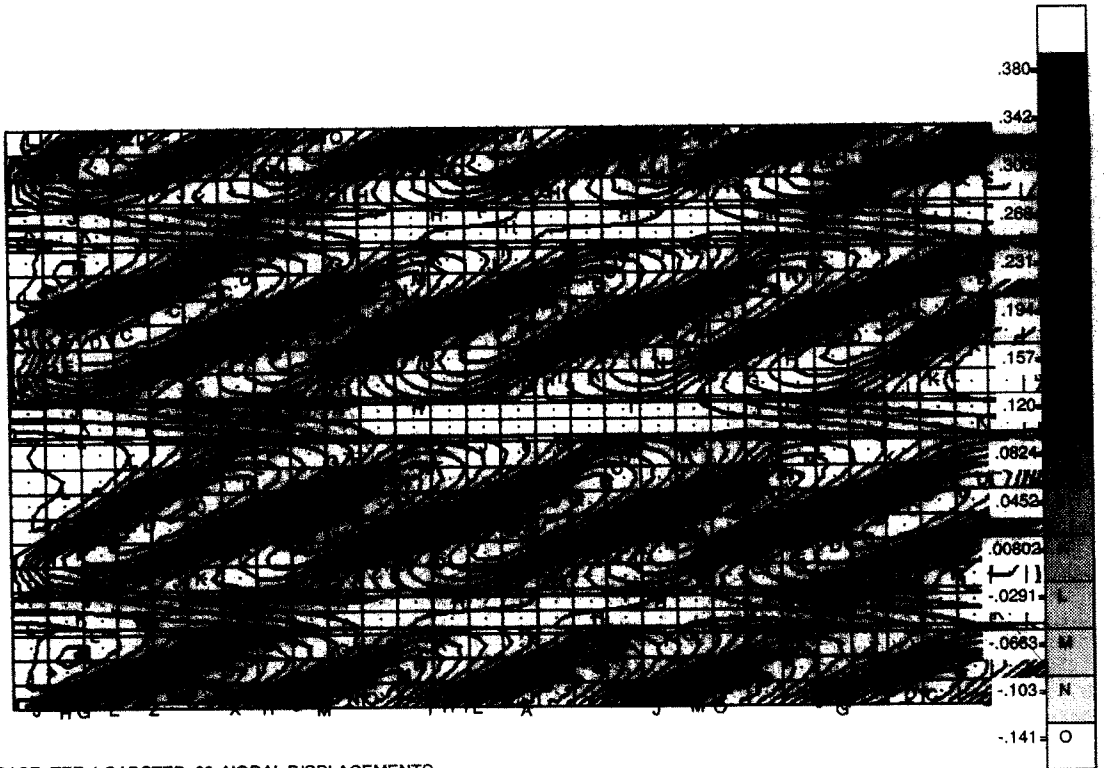

Fig. 30. Contours of normal displacement w at the design load factor $PA = 1.0$.

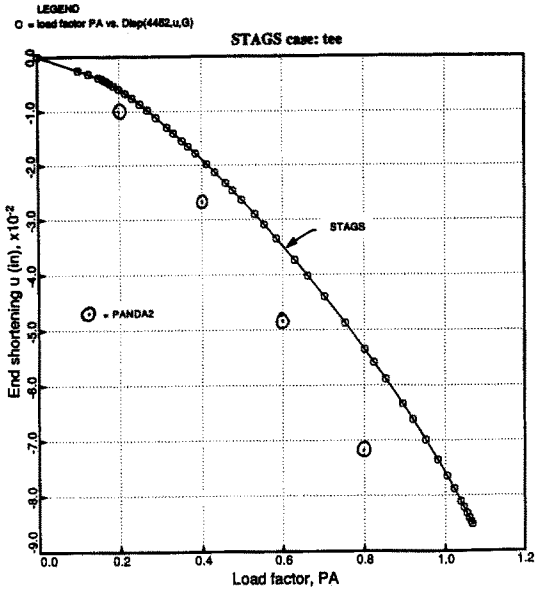

Fig. 31. Comparison of PANDA2 and STAGS predictions of end shortening. Note: the PANDA2 prediction corresponds to conditions at the panel midlength only, and therefore exceeds the STAGS prediction.

corresponds to a higher critical load factor in this case. This approach leads to safe designs because the factor of safety applied to the bending–torsion mode of buckling is the same as that used for general instability.

Figure 22 shows all design margins less than unity as functions of the loading. At the design load, $N_x = -500$ lb/in, $N_{xy} = 500$ lb/in, $p = 5.0$ psi, there are, according to PANDA2, five margins that are critical or nearly so.

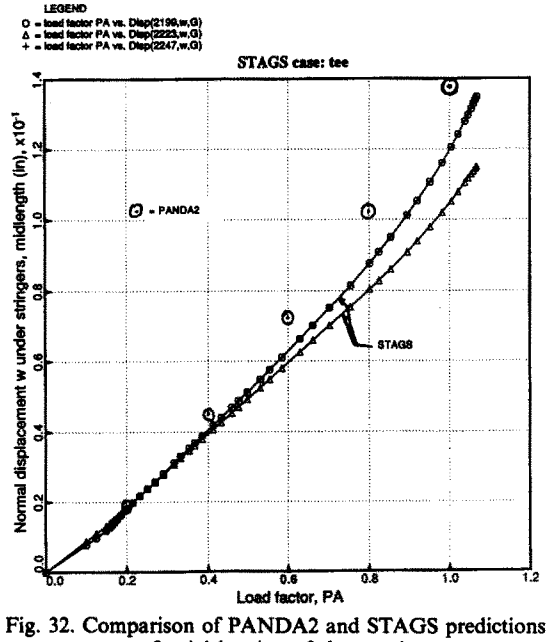

Fig. 32. Comparison of PANDA2 and STAGS predictions of axial bowing of the panel.

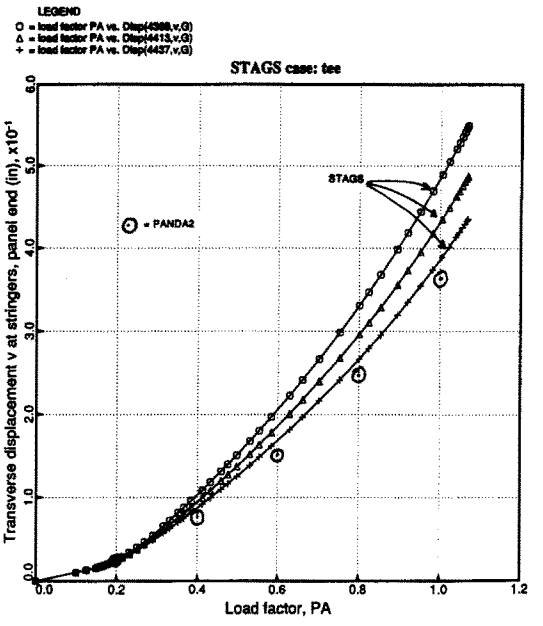

Fig. 33. Comparison of PANDA2 and STAGS predictions of overall average in-plane shearing of the panel. [Average in-plane shear strain is equal to the average transverse (hoop) displacement v at the panel end divided by the length of the panel.]

VERIFICATION WITH USE OF THE STAGS COMPUTER PROGRAM

Input data for STAGSMODEL and boundary conditions

Table 15 of [57] lists the input data for the STAGSMODEL processor, which generates input data files for the STAGS computer program. In this

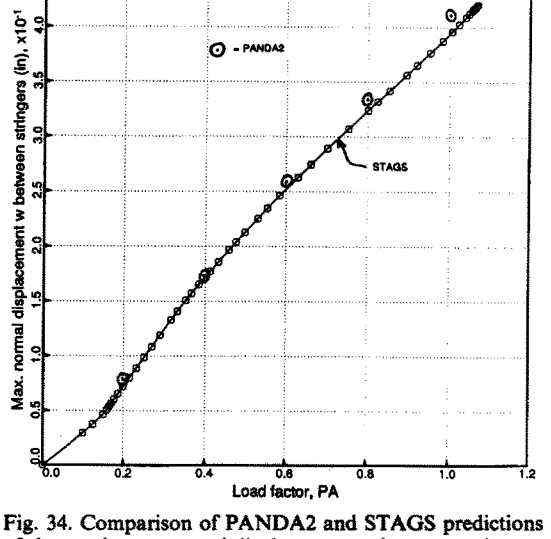

Fig. 34. Comparison of PANDA2 and STAGS predictions of the maximum normal displacement w between stringers. The maximum w as predicted by PANDA2 is the sum of w from axial bowing, w from local postbuckling, and w from the local 'pillowing' caused by normal pressure.

case STAGSMODEL is used to create a finite element model of a T-stiffened panel with three modules. Warping of the two edges parallel to the stringers in the plane of the panel skin is *not* permitted. The spacing of the stringers and thicknesses and widths of the various segments of the structure represent the optimum design generated by PANDA2. Therefore, the panel is $3 \times 5.5 = 16.5$ in wide rather than 24 in wide as shown in Fig. 6. However, the fact that three rather than four or five modules are used should not be too significant in this case, since the boundary conditions applied along the two longitudinal edges, discussed below, permit wide column buckling and simulate in an approximate way continuation of the panel in the width direction.

Figures 23 and 24(a) display the finite element model generated by STAGSMODEL and STAGS. The finite elements are of the '480' type [51, 54–56], nine-node elements that include transverse shear deformation. Each nodal point has six degrees of freedom: u, v, w, (r_u), (r_v), (r_w). The quantities (r_u), (r_v), (r_w). The quantities (r_u), (r_v), (r_w) are the rotations about the global X, Y, Z axes, respectively.

Figure 23 shows a plan view of the panel as deformed by the in-plane loads N_x, N_{xy} and the normal pressure p. Sidesway of the three stringers is permitted at the axially loaded ends of the panel, but the cross sections of the stringers cannot warp or rotate about the Y-axis at these ends. The boundary conditions imposed by the STAGSMODEL processor in this particular case are depicted in Fig. 23. If the panel has three or more stringers the degrees of freedom w, (r_u), (r_v), (r_w) at all of the nodal points along the edge $Y = 0$ are set equal to the corresponding degrees of freedom at all of the nodal points along the midbay line labelled a two bays to the left; the degrees of freedom w, (r_u), (r_v), (r_w) at all of the nodal points along the edge $Y = Y_{max}$ ($Y_{max} = 16.5$ in in this case) are set equal to the corresponding degrees of freedom at all of the nodal points along the midbay line labelled d two bays to the right. In this way a panel of infinite width is simulated approximately.

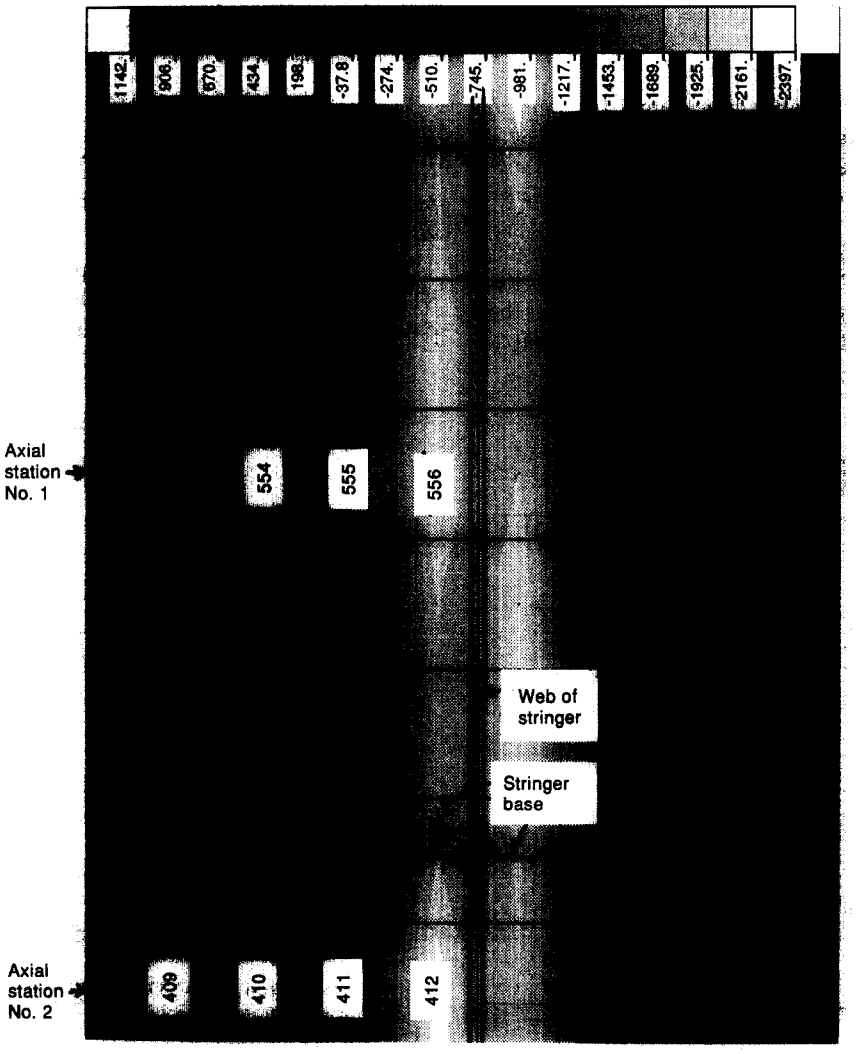

Fig. 35. STAGS prediction of the distribution of axial resultant N_x over a single panel module in the region surrounding the midlength of the panel at the design load $PA = 1.0$.

If there are less than three stringers the constraint $(r_u) = 0$ is imposed at all the nodal points along the two longitudinal edges and w, (r_v), and (r_w) are free. This edge condition is analogous to that used in PANDA2 for local and wide column buckling and is identical for panels in which the local buckling and postbuckling nodal lines are parallel to the X and Y axes (no in-plane shear loading or anisotropic effects).

The axial displacement u is forced to be uniform over the entire cross-section at the end $X = L$ and $u = 0$ over the entire cross-section at the end $X = 0$. The transverse (or circumferential or 'hoop') displacement v is forced to vary linearly along the two opposite longitudinal edges in this example because the user selected '1' in response to the prompt, 'Edges normal to screen (0) in-plane deformable: (1) rigid' (Table 15 of [57]). Lagrange constraints are used to enforce this linearity. These Lagrange constraints have the effect of almost doubling the average bandwidth of the stiffness matrix, therefore increasing the computer time required for solution by a factor of almost four over that for a panel in which warping of the two longitudinal edges is permitted in the plane of the panel skin.

Sequence of STAGSMODEL/STAGS runs required to obtain a solution

Several executions of the STAGS program are usually required in order to obtain convergence of the nonlinear behavior up to collapse of the panel or

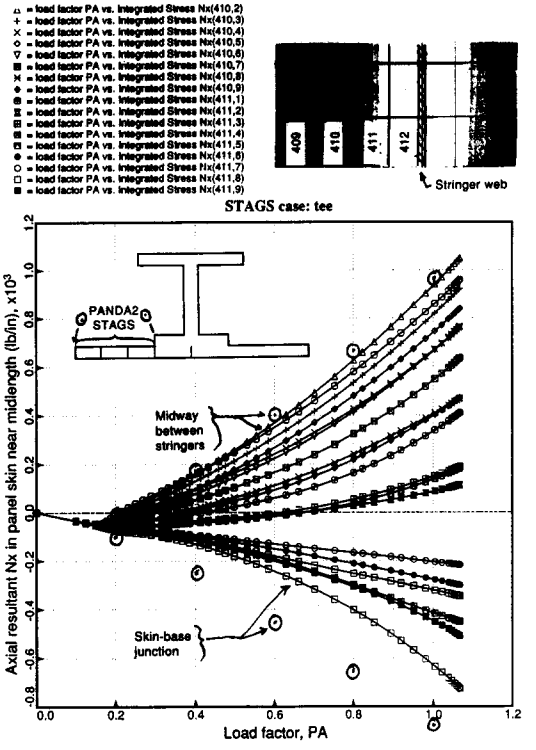

Fig. 37. Comparison of PANDA2 and STAGS predictions for the axial resultant N_x in the panel skin at axial station No. 2 indicated in Fig. 35.

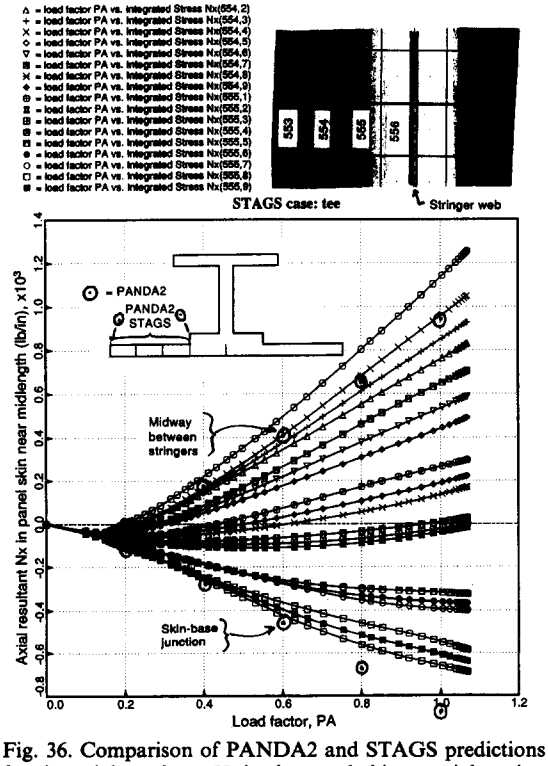

Fig. 36. Comparison of PANDA2 and STAGS predictions for the axial resultant N_x in the panel skin at axial station No. 1 indicated in Fig. 35.

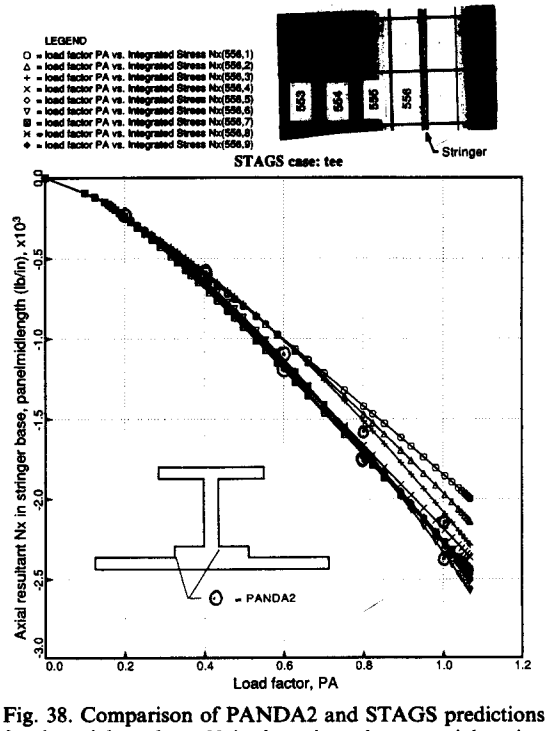

Fig. 38. Comparison of PANDA2 and STAGS predictions for the axial resultant N_x in the stringer base at axial station No. 1 indicated in Fig. 35.

beyond the design load by 10 or 20%. A typical sequence is listed in Table 2.

In this example all nonlinear (INDIC = 3) STAGS runs were performed with use of the modified Newton method. All STAGS runs were made on STARDENT's TITAN computer.

STAGS results for the three-module model with no in-plane warping of the two longitudinal edges. Figure 24(a) shows the lowest buckling mode and critical load factor, PA. The eigenvalue, LAMBDA = 0.149, agrees well with the critical buckling load factor 0.157 obtained by PANDA2 for conditions at the panel midlength (p. 2 of Table 11 in [57]). Figure 24(b) gives contours of the buckling mode in the central region of the panel. The slope of the buckling nodal lines is about 0.72. This value is plotted at the left end of the line labelled 'STAGS' in Fig. 17. There are about eight axial halfwaves in the local buckling pattern. This number is plotted at the left end of the line labelled 'STAGS' in Fig. 16. The buckling mode shown in Figs 24 (a, b) was used as an initial imperfection in the nonlinear collapse run discussed next.

Table 17 of [57] lists the input data for STAGSMODEL for setting up the first nonlinear collapse analysis of the optimized panel with STAGS. An imperfection amplitude of +0.003 in is chosen. This represents approximately ten per cent of the thickness of the optimized panel skin midway between stringers.

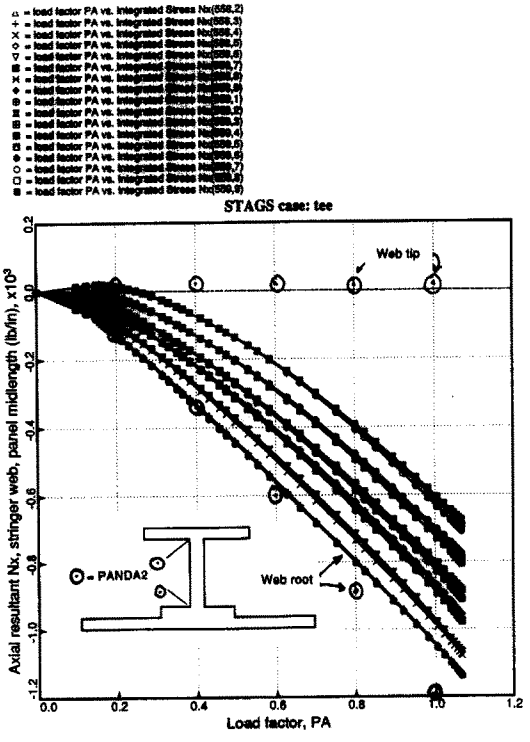

Fig. 39. Comparison of PANDA2 and STAGS predictions for the axial resultant N_x in the stringer web at axial station No. 1 indicated in Fig. 35.

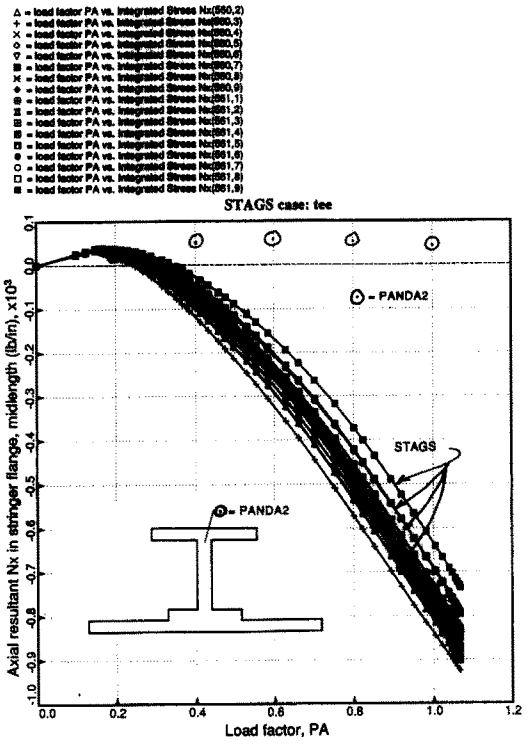

Fig. 40. Comparison of PANDA2 and STAGS predictions for the axial resultant N_x in the outstanding stringer flange at axial station No. 1 indicated in Fig. 35.

Figure 25 is a plot of load factor PA vs load step number for the first nonlinear run of the three-module model. The STAGS run could not proceed beyond load step 7 even when extremely small Riks path increments (called DETA in the STAGS output file) were used. Therefore, STAGS automatically went into an eigenvalue extraction mode at load step 7.

The prebuckled states of the panel at load factors $PA = 0.10$ and 0.17 are displayed in Figs 26(a) and (b), respectively. The 'pillowing' of the panel skin between stringers is caused by the normal pressure, which, as shown in the insert in the lower left part of Fig. 6, acts from below. The fact that the 'pillowing' is nonuniform in the axial direction arises from the presence of the initial buckling modal imperfection shown in Fig. 24(a).

Two eigenmodes and critical load factors from a nonlinear bifurcation buckling analysis for the panel as loaded by $PA = 0.1719$ (load step 7) are shown in Figs 27(a) and (b). The critical load factors, $PA = 0.17775$ corresponding to the first mode and $PA = 0.17861$ for the second, are very close to the applied load factor at load step 7, $PA = 0.1719$. This tends to confirm that it is the presence of bifurcations or near-bifurcations on the primary equilibrium path that caused the lack of convergence beyond load step 7 in the nonlinear STAGS run.

Inspection of the prebifurcation equilibrium states in Figs 26(a) and (b) reveals that it might be beneficial

to use the second mode as an imperfection shape in addition to the linear buckling mode displayed in Fig. 24(a). A negative amplitude factor applied to this second mode might be better than a positive amplitude factor because it appears from a comparison of Figs 26 (a) and (b) that the 'pillows' between adjacent stringers are 'trying' to buckle inward at two axial stations along the panel length. These 'pillows' form little cylindrical shells which, at the load factor of approximately 0.170, tend to buckle under the influence of the combined axial compression N_x and in-plane shear N_{xy}.

Table 18 of [57] lists input for STAGSMODEL used in preparation for the next nonlinear STAGS run. An amplitude factor of -0.002 is used for the imperfection shape shown in Fig. 27(b). Note that the case is restarted from the zeroth load step. Experience has shown that for problems of this type it is almost always necessary to restart the case from zero load every time a new imperfection shape is introduced via the sequence of runs described in Table 2.

Figure 28 demonstrates that inclusion of the new imperfection shape essentially eliminates the singularity on the primary equilibrium path at the load factor

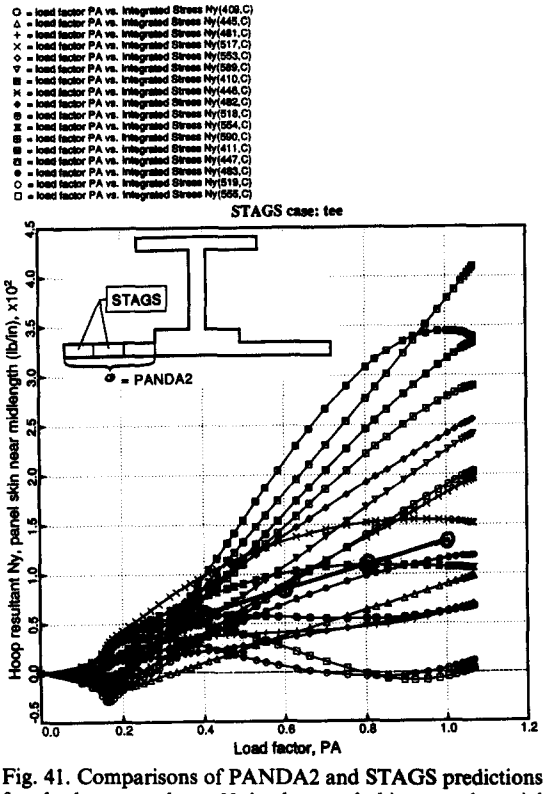

Fig. 41. Comparisons of PANDA2 and STAGS predictions for the hoop resultant N_y in the panel skin over the axial length of panel shown in Fig. 35 for the two columns of finite elements nearest the left-hand edge of the panel module. Note: the PANDA2 results are based on the assumption that N_y is constant over the entire panel skin and stringer base and that N_y is caused entirely by the uniform hoop tension generated when the panel skin 'pillows' locally between adjacent stringers when it is loaded by the uniform normal pressure.

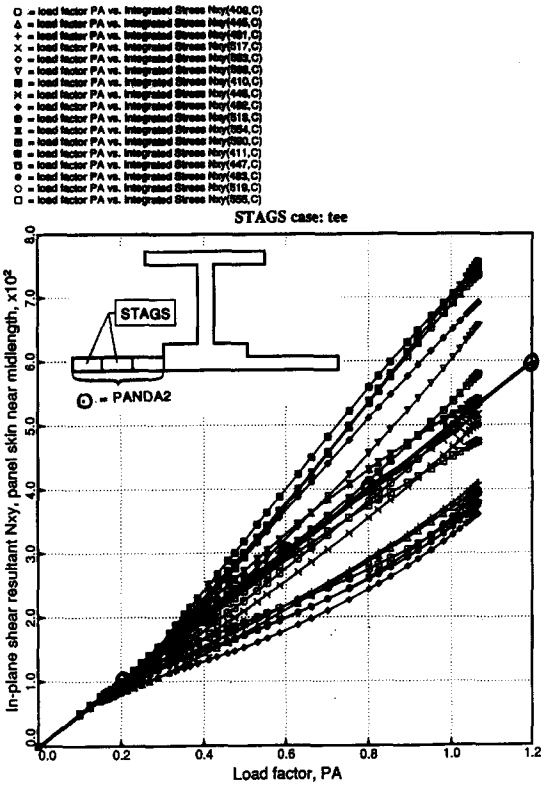

Fig. 42. Comparisons of PANDA2 and STAGS predictions for the in-plane shear resultant N_{xy} in the panel skin over the axial length of panel shown in Fig. 35 for the two columns of finite elements nearest the left-hand edge of the panel module. Note: the PANDA2 results are based on the assumption that N_{xy} is constant over the entire panel skin and stringer base and is equal to the applied in-plane shear load. ($N_{xy} = 500$ lb/in at the design load factor $PA = 1.0$.)

$PA = 0.17$. The panel can now be loaded from zero load factor to a load factor higher than that corresponding to the design load $PA = 1.0$ without further difficulty. (However, about 25 h of CPU time on the STARDENT computer was required for the run!).

Figure 29 shows how the panel deforms as the load combination N_x, N_{xy}, and p is increased in proportion. Figure 30 gives contour plots of the normal displacement w at the design load factor, $PA = 1.0$. The number of axial halfwaves over the length of the panel and the slope of the nodal lines of the local buckles are plotted at the right-hand ends of the lines labelled 'STAGS' in Figs 16 and 17, respectively. These changes in the local buckle pattern as the panel is loaded further and further into the postbuckling regime are also predicted by PANDA2.

In Figs 31–34 the overall static response of the panel as predicted by STAGS and by PANDA2 are compared. The PANDA2 results plotted in these figures come directly or are derived from values listed in Table 13 of [57], which pertains to conditions at the midlength of the panel. According to Table 13 of [57], PANDA2 overestimates the end shortening. The reason for this overestimation is discussed above.

According to Fig. 32 PANDA2 predicts more overall axial bowing of the panel than does STAGS. The 'transverse' displacements v plotted in Fig. 33 are the hoop (tangential) displacements at the intersections of stringer webs and stringer bases at the top end of the panel depicted in Fig. 23. The PANDA2 points plotted in Fig. 33 are calculated by multiplying the average shear strain e_{12} (ave) listed in Table 13 of [57] by the length of the panel (30 in). The PANDA2 points plotted in Fig. 34 are calculated by adding the absolute values of the columns in Table 13 of [57] with the headings 'Maximum post-local-buckling deflection' and 'Bowing amplitude under load, WBOW'.

Figures 35–42 give the distributions of axial resultant N_x, hoop resultant N_y, and in-plane shear resultant N_{xy} in the panel at the design load (Fig. 35) and as functions of the load factor PA (Figs 36–42). Figure 35 shows the distribution of axial resultant N_x in the center module in the neighborhood of the midlength of the panel at the design load $PA = 1.0$. Note that there is some variation in N_x in the axial direction.

STAGS and PANDA2 results are compared in Figs 36–42. Figures 36 and 37 present the distributions of axial resultant N_x in the panel skin at the two axial locations indicated in Fig. 35. The PANDA2 points are identical in the two figures because the PANDA2 theory is based on the assumption that N_x is independent of the axial coordinate x In Fig. 36 the STAGS points are for the nine integration points in each of the finite element numbers 554 and 555 and for the centroid in finite element number 553. (Finite elements 553, 554, and 555 represent the thin part of the panel skin and finite element 556 represents half of the stringer base. The left edge of finite element 553 is midway between adjacent stringers. These finite elements are located at axial station No. 1 in Fig. 35.) Figure 37 is based on the analogous data at a different axial location (axial station No. 2).

Figure 38 displays the axial resultant N_x in the stringer base, Fig. 39 shows N_x in the stringer web, and Fig. 40 gives N_x in the stringer outstanding flange. Note that PANDA2 predicts a very small axial tension at the intersection of web and outstanding flange and in the outstanding flange, whereas STAGS predicts compression. This difference arises from the fact that PANDA2 predicts more axial bowing than does STAGS. (See Fig. 32.) This error arises mainly from the effort to make PANDA2 err on the conservative side for conditions at the panel skin, where important postbuckling stresses develop.

Figures 41 and 42 show the variation of hoop resultant N_y and in-plane shear resultant N_{xy} in the panel skin with load factor PA and location along the axis of the panel. The finite elements listed in the legends are in the second and third columns from the

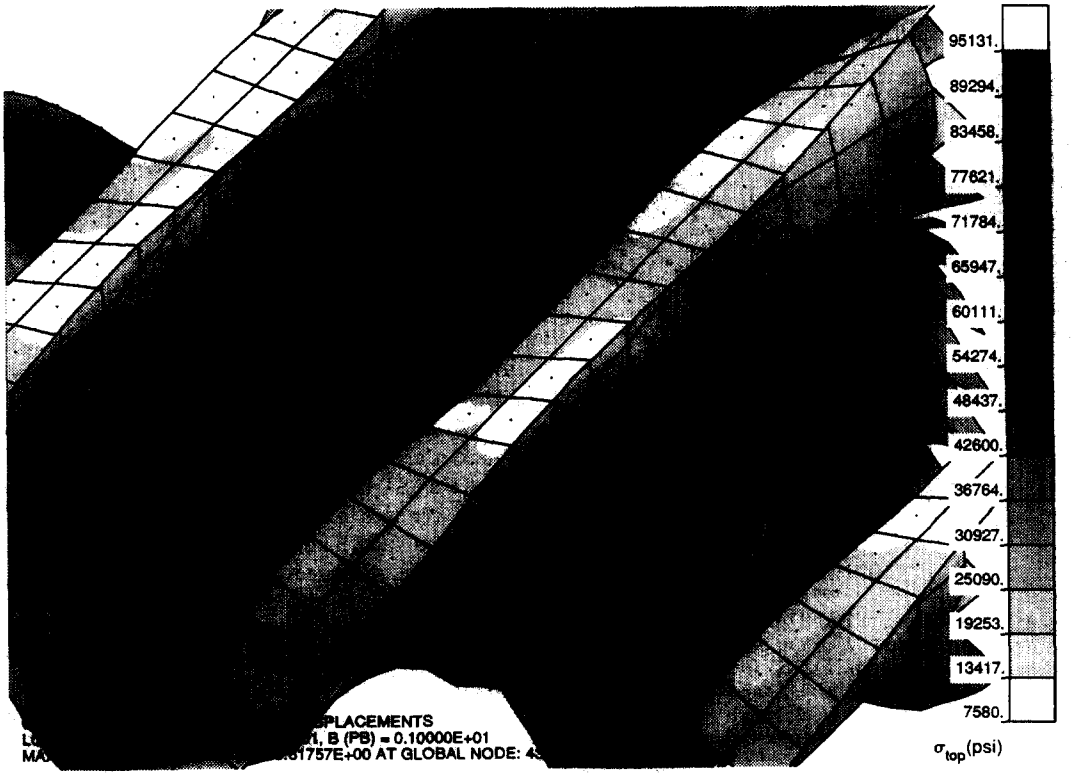

Fig. 43. PATRAN plot of the effective stress in the top fiber of the panel skin in part of the panel surrounding the midlength as predicted from the STAGS model as loaded at the design load factor $PA = 1.0$.

Fig. 44. Plan view of the region where the maximum effective stress in the top fiber of the panel skin occurs. The maximum effective stress is located in finite element 373.

left side of Fig. 35. The STAGS points correspond to the values at the centroids of these elements. In the PANDA2 analysis both N_y and N_{xy} are assumed to be constant over the entire surface of the panel skin. The hoop resultant N_y in PANDA2 arises solely from the development of hoop tension as the panel skin is loaded by normal pressure and forms 'pillows' of the type shown in Fig. 26(a), but uniform in the axial

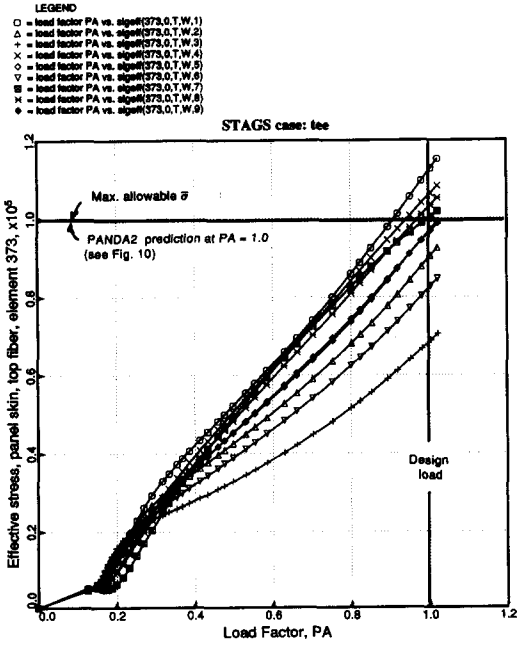

Fig. 45. Effective stress in the top fiber at the nine integration points in finite element 373 plotted vs the load factor PA.

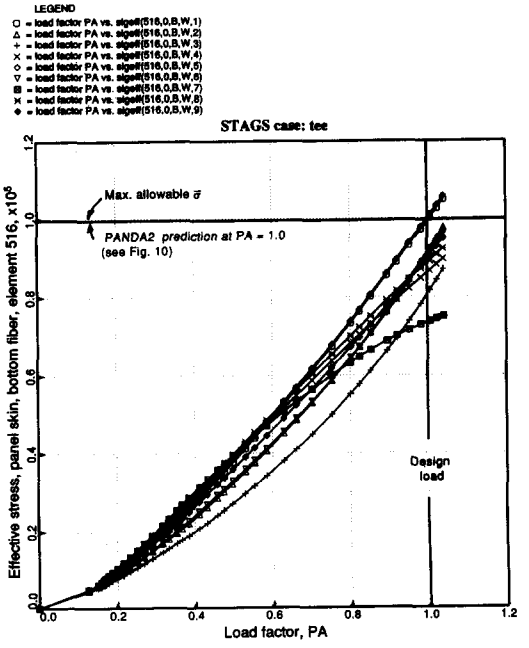

Fig. 46. Effective stress in the bottom fiber at the nine integration points in finite element 516 plotted vs the load factor PA.

direction as described in Fig. 56 of [38]. The variation of N_y over the surface of the panel skin predicted by STAGS arises from the growth of local buckles. The in-plane shear resultant N_{xy} in PANDA2 arises solely from the applied load, which is given by $N_{xy} = 500$ lb/in at the design load factor $PA = 1.0$.

Of particular interest in panels designed for operation in the post-local-buckling regime is the prediction of maximum effective (von Mises) stress. The PATRAN postprocessor [49] yields Figs 43 and 44, in which the maximum effective stress not located in the immediate neighborhood of the panel ends is predicted to be about 95,000 psi at the design load factor $PA = 1.0$. This maximum is located at the top fiber in finite element 373.

The PATRAN effective stresses represent averages of nodal point values extrapolated from the integration points within the elements in the immediate neighborhood of finite element 373 and finite element 373 itself. The averaging technique tends to cut down peaks and raise valleys. Therefore, the PATRAN display underestimates the maximum effective stress.

Figures 45 and 46 display the effective stresses in the top and bottom fibers, respectively, at the integration points in the finite elements that PATRAN indicates contain the maxima at the design load factor $PA = 1.0$. The PANDA2 result corresponds to 100 ksi at the design load factor $PA = 1.0$ because the effective stress margin is critical for conditions at the midlength of the panel, as can be seen from a careful inspection of the margins plotted at the extreme right-hand side of Fig. 10 (margins for the final design iteration, which represents the optimum design in this case). In this case PANDA2 underestimates the maximum effective stress by about 12%.

STAGS results for the three-module model with in-plane warping of the two longitudinal edges permitted. Figures 47 and 48 show some results. As expected, if in-plane warping of the two longitudinal edges is permitted, the local buckles at the design load $PA = 1.0$ are deeper than those shown in Fig. 29 for the no-warping case because the two longitudinal edges are free to move inward in the midlength region. This results in much higher local bending stresses. In Fig. 47 plan views of the post-local-buckling deformations for the no-warping case (a) and warping case (b) are compared. While the phenomenon in the no-warping case might be called 'post-buckling' that in the warping case almost has to be called 'wrinkling'.

Figure 48 is a PATRAN plot of the effective stress in the top fiber of the panel skin at the design load $PA = 1.0$ for the case in which in-plane warping of

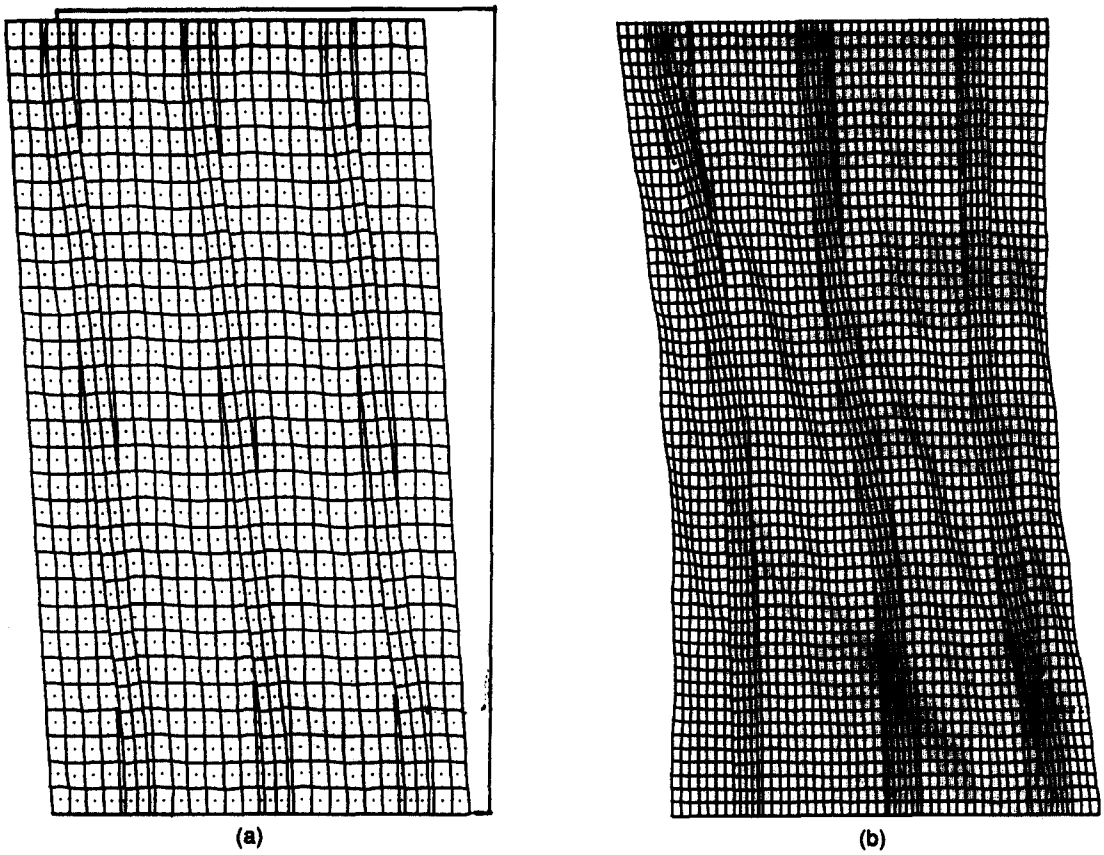

Fig. 47. Comparison of in-plane deformations at and near the design load factor $PA = 1.0$ for (a) panel in which in-plane warping of the two edges parallel to the stringers is prevented and (b) panel in which in-plane warping of these two edges is permitted.

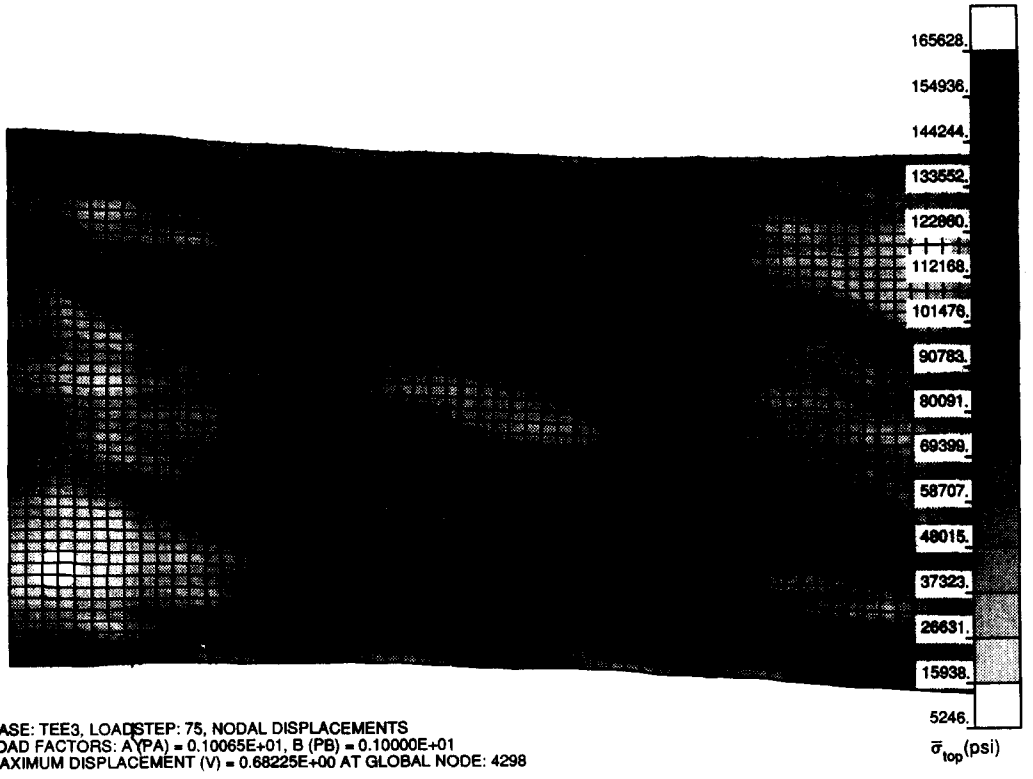

Fig. 48. PATRAN plot of the effective stress in the top fiber of the panel skin at the design load $PA = 1.0$ for a panel in which in-plane warping of the two edges parallel to the stringers is permitted.

the two longitudinal edges is permitted. The fringe values listed in this figure should be compared to the fringe values listed in Fig. 43, which pertains to the no-warping case.

These results indicate that for comparison with PANDA2, the 'no edge warping' option should be used in the STAGSMODEL processor.

CONCLUSIONS AND SUGGESTIONS FOR FURTHER WORK

Conclusions

The production of a PANDA2 processor called STAGSMODEL makes it easy to produce input files for the general-purpose nonlinear finite element program STAGS. In this way panels optimized by PANDA2 can be 'tested' by STAGS.

The agreement of predictions by PANDA2 and STAGS for the behavior of the T-stiffened panel loaded by axial compression, in-plane shear, and normal pressure far into the postbuckling regime appears to be good enough to qualify PANDA2 as a tool for the preliminary design of lightweight stiffened panels.

The following points are emphasized:

1. A sequence of STAGSMODEL/STAGS runs is required in order to complete a nonlinear collapse analysis. The sequence includes linear and nonlinear bifurcation analyses and nonlinear equilibrium analyses of imperfect configuration in which imperfections in the form of buckling modes are accumulated in order to remove singular behavior from the nonlinear equilibrium analyses.

2. For comparisons with PANDA2 the option in STAGSMODEL in which the user chooses whether or not to permit warping of the two longitudinal edges in the plane of the panel skin should be set to 'no warping'.

3. The user should obtain plots of critical values such as effective stress at the integration points of the finite elements where PATRAN predicts the maximum values to occur. PATRAN tends to underestimate critical values, which it 'smooths' by averaging.

Suggestions for further work

Further numerical work.

1. A large number of simpler cases (such as flat, unstiffened plates under various combination of axial compression and in-plane shear loading) should be explored in order to test further the reliability of the sequence of STAGSMODEL/STAGS runs suggested in Table 2 and used for the analysis of the T-stiffened panel.

2. Numerical models of the T-stiffened panel fabricated from laminated composite materials should be optimized with PANDA2 and the optimum designs checked with STAGS.

Suggested enhancements of STAGS. The following is a list of suggestions for STAGS enhancements

which would make it easier to use STAGS for 'testing' stiffened, composite panels designed via PANDA2.

1. Introduce an adaptive refinement strategy in STAGS in which the user is free to choose a region or regions both in the model and in the load space in which he/she wants the strategy switched on or off. The cases explored here, being highly nonlinear, require several restarts and many load steps. Yet the stresses vary rapidly in certain areas. It would be advantageous to be able to concentrate nodes in these areas in an automated way.

2. Improvements are needed in the stepping strategy for nonlinear analysis:

(a) Try to do something to counteract the tendency of the Riks path to turn back upon itself. Often, when the step size gets small, the Riks method converges to a previous solution at a lower load. From then on the panel unloads along the primary path, rather than loading further into the nonlinear postbuckled regime as is desired.
(b) Under certain circumstances cut the step size if roots have been skipped.
(c) Allow the user to supply a maximum allowable step size. Sometimes the step size gets too big, and details of the nonlinear behavior are missed.
(d) Permit run termination when max. displacement, end shortening, stress, strain, or other user-specified quantity exceeds a user-supplied value.

3. Include a more general material law for transverse shear deformation (TSD). As the program stands now, only $G12$ (in-plane shear modulus) is provided by the user and $G13$, $G23$ are derived from the modulus transverse to the fibers and the major Poisson ratio.

4. As a long-term goal it would be ideal for STAGS to perform a sequence of computations such as listed in Table 2 in an automated fashion. If the step size becomes very small, STAGS would automatically invoke the nonlinear bifurcation branch, adding another imperfection shape (with automatically supplied amplitude!) in order to remove the near singularity from the nonlinear load–displacement path.

Acknowledgements—The first author wishes to express his appreciation for the continuing support of Mr Stan Simson and Mr Bill Sable, Stress and Fractural Mechanics department in Lockheed Missiles and Space Company's Satellite Systems Division. The authors are indeed grateful to Frank Brogran and Charles Rankin, the developers of STAGS, for their contributions to the creation of the STAGS postprocessor STAGSPP, for their quick responses to requests for modifications in STAGS, and for their patience in teaching the first author how to use STAGS and how to write the processor STAGSMODEL in order to avoid possible numerical difficulties, especially those associated with boundary conditions. The authors also wish to thank Harold Cabiness for his contributions to STAGSPP and for his forbearance, especially with the senior author, in spending considerable time to introduce PATRAN to a person who remains uneasy when confronted with user's manuals with more than a few pages.

REFERENCES

1. A. W. Leissa, Buckling of laminated composite plates and shell panels. AFWAL-TR-85-3069, Air Force Wright Aeronautical Laboratories, Wright-Patterson AFB (1985).
2. J. F. M. Wiggenraad, Postbuckling of thin-walled composite structures—design, analysis, and experimental verification. National Aerospace Laboratory (NLR), The Netherlands, Memorandum SC-86-013 U (1986).
3. R. R. Arnold and J. C. Parekh, Buckling, postbuckling, and failure of flat and shallow-curved, edge-stiffened composite plates subject to combined axial compression and shear loads. Presented at *27th SDM Meeting*, San Antonio, TX, April 1986, AIAA Paper No. 86-1027-CP, pp. 769–782 (1986).
4. D. Bushnell, PANDA-interactive program for minimum weight design of stiffened cylindrical panels and shells. *Comput. Struct.* **16**, 167–185 (1983).
5. D. Bushnell, Theoretical basis of the PANDA computer program for preliminary design of stiffened panels under combined in-plane loads. *Comput. Struct.* **27**, 541–563 (1987).
6. D. Bushnell, *Computerized Buckling Analysis of Shells*. M. Nijhoff (1985).
7. M. Baruch and J. Singer, Effect of eccentricity of stiffeners on the general instability of stiffened cylindrical shells under hydrostatic pressure. *J. Mech. Engng Sci.* **5**, 23–27 (1963).
8. J. H. Starnes, Jr, N. F. Knight, Jr and M. Rouse, Postbuckling behavior of selected flat stiffened graphite–epoxy panels loaded in compression. AIAA Paper 82-0777, presented at *AIAA 23rd Structures, Structural Dynamics, and Materials Conference*, New Orleans (1982). See *AIAA Jnl* **23**, 1236–1246 (1985).
9. E. E. Spier, On experimental versus theoretical incipient buckling of narrow graphite/epoxy plates in compression. *Proc. AIAA 21st SDM Conference*, AIAA Paper 80-0686-CP (1980).
10. E. E. Spier, Local buckling, postbuckling, and crippling behavior of graphite–epoxy short thin-walled compression members. Naval Air Systems Command, Washington, DC, NASC-N00019-80-C-0174 (1981).
11. M. P. Renieri and R. A. Garrett, Investigation of the local buckling, postbuckling and crippling behavior of graphite/epoxy short thin-walled compression members. McDonnell Douglas Corporation, St Louis, Missouri, MDC A7091 (1981).
12. M. P. Renieri and R. A. Garrett, Postbuckling fatigue behavior of flat stiffened graphite/epoxy panels under shear loading. Naval Air Development Center, Warminster, PA, NADC-81-168-60 (1982).
13. L. W. Rehfield and A. D. Reddy, Observations on compressive local buckling, postbuckling, and crippling of graphite/epoxy airframe structure. *Proc. 27th AIAA SDM Conference*, AIAA Paper 86-0923-CP (1986).
14. T. Weller, G. Messer and A. Libai, Repeated buckling of graphite epoxy shear panels with bonded metal stiffeners. Department of Aeronautical Engineering, Technion, Haifa, Israel, TAE No. 546 (1984).
15. B. L. Agarwal, Postbuckling behavior of composite, stiffened, curved panels loaded in compression. *Experimental Mechanics* **22**, June (1982).
16. C. Blaas and J. F. M. Wiggenraad, Development and test verification of the ARIANE 4 interstage 2/3 in

CFRP. *Proceedings of the AIAA/ASME 27th Structures, Structural Dynamics and Materials Conference*, Part 1, pp. 307–313 (1986).
17. J. M. T. Thompson, J. D. Tulk and A. C. Walker, An experimental study of imperfection-sensitivity in the interactive buckling of stiffened plates. In *Buckling of Structures* (Edited by B. Budiansky), Springer, pp. 149–159 (1979).
18. D. Bushnell, A. M. C. Holmes, D. L. Flaggs and P. J. McCormick, Optimum design, fabrication, and test of graphite–epoxy, curved, stiffened, locally buckled panels loaded in axial compression. In *Buckling of Structures* (Edited by I. Elishakoff *et al.*), pp. 61–131. Elsevier, Amsterdam (1988).
19. N. R. Bauld, Jr and N. S. Khot, A numerical and experimental investigation of the buckling behavior of composite panels. *Comput. Struct.* **15**, pp. 393–403 (1982).
20. N. S. Khot and N. R. Bauld, Jr, Further comparison of the numerical and experimental buckling behaviors of composite panels. *Comput. Struct.* **17**, 61–68 (1983).
21. Y. Zhang and F. L. Matthews, Postbuckling behavior of anisotropic laminated plates under pure shear and shear combined with compressive loading. *AIAA Jnl* **22**, 281–286 (1984).
22. B. O. Almroth and F. A. Brogan, The STAGS computer code. NASA CR-2950, NASA Langley Research Center, Hampton, VA (1978).
23. C. C. Rankin, P. Stehlin and F. A. Brogan, Enhancements to the STAGS computer code. NASA CR 4000, NASA Langley Research Center, Hampton, VA (1986). G. A. Thurston, F. A. Brogan and P. Stehlin, Postbuckling analysis using a general purpose code. *AIAA Jnl* **24**, 1013–1020 (1986).
24. T. R. Graves-Smith and S. Sridharan, A finite strip method for the post-locally-buckled analysis of plate structures. *Int. J. Mech. Sci.* **20**, 833–843 (1978).
25. F. Stoll and Z. Gürdal. Nonlinear analysis of compressively loaded linked-plate structures. AIAA Paper 90-0968-CP, *Proceedings 31st AIAA/ASME Structures, Structural Dynamics, and Materials Meeting*, pp. 903–913 (1990).
26. F. Stoll, Z. Gürdal and H. J. Starnes Jr, A method for the geometrically nonlinear analysis of compressively loaded prismatic composite structures. VIPSU Center for Composite Materials and Structures Report CCMS-91-03 (VPI-E-91-01) (1991).
27. D. K. Shin, Z. Gürdal and O. H. Griffin, Jr, Minimum weight design of laminated composite plates for postbuckling performance. AIAA Paper 91-0969-CP, *Proceedings 32nd AIAA/ASME Structures, Structural Dynamics, and Materials Meeting*, pp. 257–266 (1991).
28. E. Riks, A finite strip method for the buckling and postbuckling analysis of stiffened panels in wing box structures. National Aerospace Laboratory (NLR), Report NLR CR 89383 L, The Netherlands (1989).
29. M. S. Anderson and W. J. Stroud, General panel sizing computer code and its application to composite structural panels. *AIAA Jnl* **17**, 892–897 (1979).
30. W. J. Stroud and M. S. Anderson, PASCO: Structural panel analysis and sizing code, capability and analytical foundations. NASA TM-80181, NASA Langley Research Center, Hampton, VA (1981).
31. W. J. Stroud, W. H. Greene and M. S. Anderson, Buckling loads of stiffened panels subjected to combined longitudinal compression and shear: results obtained with PASCO, EAL, and STAGS computer programs. NASA TP 2215, NASA Langley Research Center, Hampton, VA (1984).
32. J. N. Dickson, R. T. Cole and J. T. S. Wang, Design of stiffened composite panels in the post-buckling range. In *Fibrous Composites in Structural Design* (Edited by E. M. Lenoe, D. W. Oplinger and J. J. Burke), pp. 313–327. Plenum Press, New York (1980).
33. J. N. Dickson, S. B. Biggers and J. T. S. Wang, Preliminary design procedure for composite panels with open-section stiffeners loaded in the post-buckling range. In *Advances in Composite Materials* (Edited by A. R. Bunsell *et al.*), pp. 812–825. Pergamon Press, Oxford (1980).
34. J. N. Dickson and S. B. Biggers, POSTOP: Postbuckled open-stiffened optimum panels, theory and capability. NASA Langley Research Center, Hampton, VA, NASA Contractor Report from NASA Contract NAS1-15949 (1982).
35. R. Butler and F. W. Williams, Optimum design features of VICONOPT, an exact buckling program for prismatic assemblies of anisotropic plates. AIAA Paper 90-1068-CP, *Proceedings 31st AIAA/ASME Structures, Structural Dynamics, and AIAA/ASME Structures, Structural Dynamics, and Materials Meeting*, pp. 1289–1299.
36. F. W. Williams, D. Kennedy and M. S. Anderson, Analysis features of VICONOPT, an exact buckling and vibration program for prismatic assemblies of anisotropic plates. AIAA Paper 90-0970-CP, *Proceedings 31st AIAA/ASME Structures, Structural Dynamics, and Materials Meeting*, pp. 920–929.
37. M.-H. Peng and S. Sridharan, Optimized design of stiffened panels subject to interactive buckling. AIAA Paper 90-1067-CP, *Proceedings 31st AIAA/ASME Structures, Structural Dynamics, and Materials Meeting*, pp. 1279–1288.
38. D. Bushnell, PANDA2-Program for minimum weight design of stiffened, composite, locally buckled panels. *Comput. Struct.* **25**, 469–605 (1987). See also, D. Bushnell, Optimization of composite, stiffened, imperfect, panels under combined loads for service in the postbuckling regime. *Comput. Meth. Appl. Mech. Engng* **103**, 43–114 (1993).
39. G. N. Vanderplaats, CONMIN—a FORTRAN program for constrained function minimization. NASA TM X 62-282, version updated in March, 1975, Ames Research Center, Moffett Field, CA (1973). See also, G. N. Vanderplaats and F. Moses, Structural optimization by methods of feasible directions. *Comput. Struct.* **3**, 739–755 (1973).
40. G. N. Vanderplaats, ADS—a FORTRAN program for automated design synthesis, Version 2.01, Engineering Design Optimization, Inc, Santa Barbara, CA (1987).
41. G. N. Vanderplaats and H. Sugimoto, A general-purpose optimization program for engineering design. *Comp. Struct.* **24**, 13–21 (1986).
42. D. Bushnell, BOSOR4: program for stress, buckling, and vibration of complex shells of revolution. *Structural Mechanics Software Series*, Vol. 1 (Edited by N. Perrone and W. Pilkey). University Press of Virginia, Charlottesville, VA (1977). See also *Comput. Struct.* **4**, 399–435 (1974). *AIAA Jnl.* **9**, 2004–2013 (1971). *Structural Analysis Systems*, Vol. 2 (Edited by A. Niku-Lari), pp. 25–54. Pergamon Press, Oxford (1986). *Comput. Struct.* **18**, 471–536 (1984).
43. W. T. Koiter, Het schuifplooiveld by grote overshrijdingen van de knikspanning. Nationaal Luchtsvaart Laboratorium, The Netherlands, Report X295 (1946).
44. D. Bushnell. Improvements to PANDA2. Unpublished literature distributed with PANDA2 (1991–1992).
45. D. Bushnell, PANDA2.NEWS. Unpublished literature distributed with PANDA2. Also a PANDA2 file that is kept up-to-date (1991).
46. D. Bushnell, Truss-core sandwich design via PANDA2, *Comput. Struct.* **44**, 1091–1119 (1992).
47. D. Bushnell, Optimization of a Tee-stiffened panel under axial compression, in-plane shear, and normal

pressure. AIAA Paper 91-1207-CP. *Proceedings 32nd AIAA/ASME Structures, Structural Dynamics, and Materials Meeting*, pp. 588–611.
48. R. J. Roark and W. C. Young. *Formulas for Stress and Strain*, 5th Edn, in particular Table 10, p. 158, Formula 2d. McGraw-Hill (1975).
49. PATRAN-Plus user manual, Release 2.4, PDA Engineering, Costa Mesa, CA (1989).
50. C. C. Rankin and F. A. Brogan, An element independent corotational procedure for the treatment of large rotations. *J. Pressure Vessel Technol.* **108**, 165–174 (1986).
51. F. A. Brogan, C. C. Rankin and H. D. Cabines, STAGS user's manual. Lockheed Missiles and Space Co. Report LMSC P032594, Dec. (1993).
52. F. A. Brogan, W. D. Bushnell, H. Cabiness and C. Rankin, STAGSPP, a postprocessor for STAGS (not yet released).
53. D. Bushnell, Annotated output from PANDA2 mainprocessor for a fixed design. Unpublished literature for PANDA2.
54. G. M. Stanley. Continuum-based shell elements, Ph.D. dissertation, Stanford University, Stanford, CA (1985).
55. K. C. Park and G. M. Stanley, A curved C_0 shell element based on assumed natural coordinate strains. *J. Appl. Mech.* **108**, 278–290 (1986).
56. G. M. Stanley, K. C. Park and H. Cabiness, The computational structural mechanics testbed structural element processor ES7: Revised ANS shell elements. NASA CR 4360, NASA Langley Research Center (1991).
57. D. Bushnell and W. D. Bushnell, Minimum-weight design of a stiffened panel via PANDA2 and evaluation of the optimized panel via STAGS. Report that contains the matter presented in this paper plus tables of the input data used for the runstream listed in Table 1.